Part II:
Mass and Age Distributions in Young Associations

Chapter 6

Age and Mass Distributions for Low Mass Members of Young Clusters and Associations[1]

Much progress has been made within the past several decades towards our understanding how isolated stars are created. In its basic form, our current view today of isolated star formation is not substantially different from that put forth by Shu et al. (1987). However, as discussed in chapter 1, most stars do not form in isolation, they form in groups, and many details of this process remain unexplained. In particular, how and why do molecular clouds contract at particular sites to form stellar groups? What determines whether a particular star formation site will become a sparse Taurus-like association, a bound cluster such as the Orion Nebula Cluster, or an expanding OB association similar to USco? Do all members of a single star-forming group form in a single burst or is star formation a lengthy process?

In this chapter, I address some of these questions by assessing the age distributions of young star-forming regions. A useful tool in understanding the distribution of ages within a group of stars is the HR diagram. Once each object's spectral type and photometry is measured, those values can be combined to derive values for its luminosity and effective temperature and place it on a theoretical HR diagram. Using theoretical pre-main sequence evolutionary tracks, temperatures and luminosities can be transformed into ages and masses. Thus, I can use the HR diagram for USco

[1] A modified version of § 6.1 has been published previously as Slesnick, Hillenbrand, & Carpenter 2004, ApJ, 610, 1045.

derived in chapter 5 to derive the age distribution for low mass members of this OB association. My survey in Taurus identified tens of previously unknown intermediate-age PMS stars (several megayears older than the known Taurus population), but the relationship of these stars to the Taurus association remains ambiguous until follow-up studies can be completed (see §4.5). Therefore I can not use an HR diagram for this population to derive ages in an equivalent manner.

However, during my time at Caltech prior to my work on the Quest-2 surveys, I carried out a study to assess the star formation history of another young star-forming region, the Orion Nebula Cluster (hereafter ONC). The ONC is an ideal region in which to address questions relating to star formation in clusters because it contains >3000 members across a range of spectral types from O stars to brown dwarfs. It is also the nearest massive cluster to the sun (∼480 pc; Genzel et al. 1981). Thus, for the remainder of this chapter, I will assess and compare the star formation histories of the USco OB association and the embedded Orion Nebula Cluster. For the purpose of this discussion, I present only the analysis section of my work in the ONC, not the full study. Observational details for this survey can be found in Slesnick et al. (2004).

Another unanswered question fundamental to the theory of star formation within a stellar group is whether the distribution of stellar masses formed during a single epoch within an association or cluster, also known as the initial mass function (IMF), is universal or whether it varies with either star formation environment or time. We believe we understand the basic structure of the field star IMF at 'normal' stellar masses above ∼0.5 $M_\odot$ and below ∼10 $M_\odot$. In this mass range the field star IMF is generally well characterized by a power law slope $dN/dM \propto M^{-2.35}$, as derived originally by Salpeter (1955). However, while the shape of the *stellar* mass function is relatively well known, we are still struggling to understand the very low mass end of the distribution into the substellar regime. For stars and brown dwarfs less massive than ∼0.4–0.5 $M_\odot$, the shape of the mass function remains ambiguous and may be strongly dependent on the environment within the parental molecular cloud. Young stellar clusters and associations are particularly valuable for examining the shape of the low mass IMF because contracting low-mass pre-main sequence stars and brown

dwarfs are 2-3.5 orders of magnitude more luminous than their counterparts on the main sequence, and thus can be more readily detected in large numbers. Furthermore, the lowest mass members of young stellar groups have not yet been lost to dynamical evolution.

In addition to discussing the age distributions of the ONC and USco populations in this chapter, I use derived HR diagrams to examine the low mass IMFs of each star forming region. I will first discuss my work in the ONC. Second, I use the HR diagram derived in chapter 5 to determine an IMF for low mass stars and brown dwarfs in the USco region. Because I do not believe that all of the new PMS stars identified near Taurus are related to the known young subgroups, I do not attempt to use these stars to derive an IMF for Taurus from my data. Instead, I compare my results for USco and the ONC to results published in the literature for Taurus and for other young regions.

6.1 Age/Mass Distributions of the Low Mass Population in the ONC

The ONC is one of the nearest massive star-forming regions to the Sun and the most populous young cluster within $\sim$2 kpc. Thus, it has been observed at virtually all wavelengths over the past several decades. However, only recently have increased sensitivities due to near-IR detectors on larger telescopes allowed us to begin to understand and characterize the extent of the ONC's low mass stellar and brown dwarf population which, at $\lesssim$ 1-2 Myr, is just beginning to emerge from its giant molecular cloud.

Several recent studies have explored the ONC at substellar masses. Hillenbrand & Carpenter (2000) (hereafter HC00) present the results of an H and K imaging survey of the inner 5'.1 x 5'.1 region of the ONC. Observed magnitudes, colors, and star counts were used to constrain the shape of the ONC mass function across the hydrogen burning limit down to $\sim$0.03 $M_{\odot}$. They find evidence in the log-log

mass function for a turnover above the hydrogen-burning limit, then a plateau into the substellar regime. A similar study by Muench et al. (2002) (hereafter M02) uses J, H, K imaging of the ONC to derive an IMF which rises to a broad primary peak at the lowest stellar masses between 0.3 $M_\odot$ and the hydrogen burning limit before turning over and declining into the substellar regime. However, instead of a plateau through the lowest masses, M02 find evidence for a secondary peak between 0.03 and 0.02 $M_\odot$. Luhman et al. (2000) use H and K infrared imaging and limited ground-based spectroscopy to constrain the mass function and find a similar peak just above the substellar regime, but then a steady decline through the lowest mass objects.

Generally speaking, J, H, K photometry alone is insufficient for deriving stellar/substellar masses, though may be adequate in a statistical sense for estimating mass distributions given the right assumptions. The position of a young star in a near-IR color-magnitude diagram (CMD) is dependent on mass, age, extinction, and the possible presence of a circumstellar disk. These characteristics affect the conversion of a star's infrared magnitude and color into its stellar mass. Unless the distributions of these parameters are known a priori, knowledge of the cluster's luminosity function alone is not sufficient to draw definitive conclusions about its mass function. In addition, cluster membership is often poorly known and statistical estimates concerning the extent and characterization of the field star population must be derived. In the case of the densely populated ONC, it has been suggested that the field star contamination is small but negligible toward fainter magnitudes. HC00 used a modified version of the Galactic star count model (Wainscoat et al., 1992) convolved with a local extinction map (derived from a $C^{18}O$ molecular line map) to estimate the field star contribution, which they found to constitute $\sim$5% of the stars down to their completeness limit at $K \sim 17.5$.

In order to study a cluster's IMF in more than just a statistical sense, spectroscopy is needed to confirm cluster membership of individual stars and uniquely determine location in the HR diagram (see chapter 3). Candidate substellar objects were selected from the HC00 photometric survey for follow-up spectroscopy to determine if their temperatures and surface gravities are consistent with those of brown dwarf objects

at the age and distance of the ONC. I, along with Lynne Hillenbrand and John Carpenter, obtained new infrared spectra of 97 objects within the ONC; 81 selected from the HC00 work were observed using NIRSPEC and 16 selected from the optical magnitudes and colors of Hillenbrand (1997) (hereafter H97) were observed using CRSP. The sample included ∼50% of the stars in the HC00 survey area expected to be brown dwarfs based on their $K, (H-K)$ magnitudes and colors, down to the completeness limit of K ∼17.5. From the NIRSPEC data, I classified 71 objects in the inner ONC found to be of spectral type K7 or later, ∼50% of which are M6 or later. At an age of 1-2 Myr, all objects with spectral types later than M6 are substellar (M < 0.08 $M_\odot$) based on comparison with theoretical models (e.g., D'Antona & Mazzitelli 1997; hereafter DM97). In addition, 16 spectra of objects in the inner and outer parts of the nebula were taken with CRSP, 9 of which were classified M6 or later. A few spectral types from new optical LRIS data are also included in this analysis.

6.1.1 HR Diagram for Substellar Objects in the ONC

In figure 6.1 I present an HR diagram for those objects within the inner 5.'1 × 5.'1 of the ONC (survey area of HC00) for which new spectral types were obtained. Surface gravity assessment is indicated and a typical error bar for an M6±1.5 star is shown in the lower left corner. The pre-main-sequence model tracks and isochrones of DM97 are also shown. Figure 6.1 illustrates that this survey probes lower masses than previous spectroscopic studies have, down to 0.02 $M_\odot$.

From examination of figure 6.1, it appears that this survey explored two separate populations: the inner ONC at $\lesssim$1 Myr, and an older population at ∼10 Myr. None of the members of this apparently older population have gravity features which indicate they might be foreground M stars. Spectra of these objects indicate instead that they have low surface gravity consistent with young objects, and are therefore also candidate cluster members. For the remainder of §6.1.1, I discuss the possible explanations for this surprising population. First, I detail possible systematics in the data reduction/analysis which could, in principle, cause one to "create" older stars

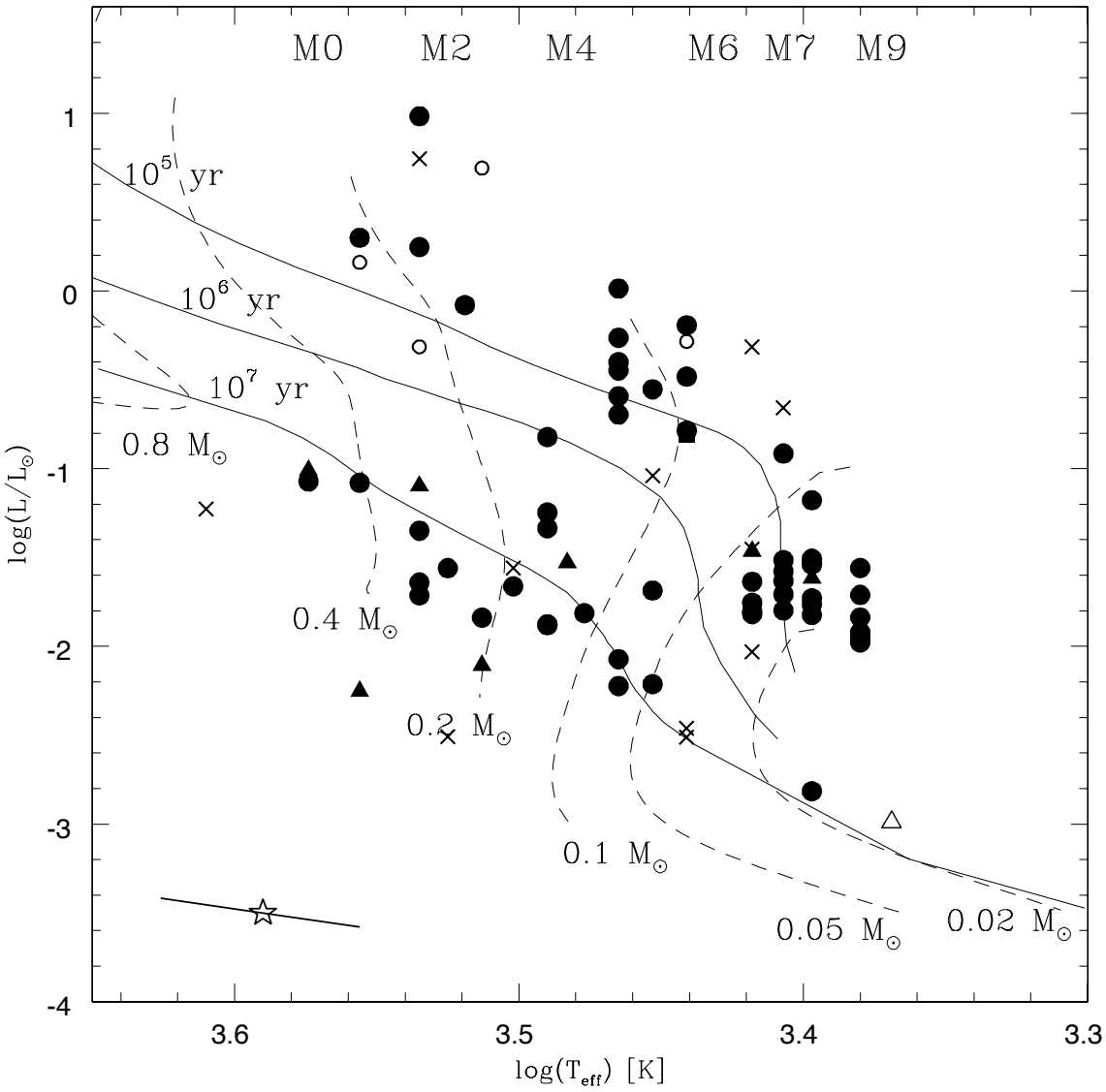

Figure 6.1 HR diagram of objects within the inner 5.'1 × 5.'1 of the ONC (survey area of HC00) for which I have new spectral types. Filled symbols correspond to stars classified using NIRSPEC and CRSP infrared observations which have good spectral types. Objects that were classified as "high" gravity (i.e., had strong absorption lines, similar in strength to dwarf stars of the same temperatures) are marked as open symbols and objects with less certain spectral types are marked as X's. Triangles represent objects which have new optical spectral types taken with LRIS. A typical error bar for an M6±1.5 star is shown in the lower left corner. The pre-main-sequence model tracks and isochrones of DM97 are also shown.

in the HR diagram. Next I discuss their possible origin if they are a real feature, and finally I determine why they may not have been detected in previous studies.

There are two possible reasons one might erroneously detect a bifurcation of the HR diagram: either the spectral types are in error and the objects are actually cooler than they are shown to be here, or their luminosities have been underestimated. A full description of how stars were placed in the HR diagram is given in Slesnick et al. (2004). The photometric uncertainties for these objects are <0.2 mag for both H, K in the HC00 data and < 0.4 mag for J, H, K in the M02 data. The two data sets agree to within 0.8 mag for all objects and variability, if present, is expected to be $\sim$0.2 mag (Carpenter et al., 2001). An object with spectral type M2 would need to be $\sim$3 magnitudes brighter in K, or have its extinction underestimated by >30 mag in order to move on the HR diagram from the 10 Myr isochrone to the 1 Myr isochrone. Even taking into account the above uncertainties and possible variability, errors of this magnitude are not possible. Moreover, if the photometry were in error, the expected result would be continuous scatter in the HR diagram, rather than two distinguishable branches.

The other way to account for the apparently older population through error is if the temperature estimates are too hot, i.e., the spectral types too early, in some cases by as much as 7 spectral subclasses. All spectra have been checked visually, by both me and my advisor Lynne Hillenbrand to ensure accurate classification, and I believe the spectral types are robust to $\pm$1 subtype. None of the possible biases resulting from assumptions made regarding veiling, extinction or gravity can have a large enough effect to produce a spectral type offset of this magnitude (see Slesnick et al. 2004). One possible exception is that a mid-M (M5) K-band spectrum with high reddening can have the same appearance and classification band index measurements as a later-M (M7) spectra with intermediate reddening. But this phenomenon could only affect a small subset of the lower branch population. Therefore, while it may reduce slightly the number of apparent older objects, it cannot correct for them entirely.

The accuracy of the spectral types is supported by the excellent agreement of the near-IR spectral classifications with existing optical spectral types, when present

(most agree to within 2 spectral subclasses). A significant fraction of the spectra taken with LRIS (filled triangles on figure 6.1), which were classified in a completely independent manner from the NIRSPEC and CRSP data, also resulted in several apparently 10 Myr old stars. If the older population arises from systematics in the reduction or spectral classification of the infrared spectra, it would not be expected that stars classified optically would fall on the same place in the HR diagram.

If we are to accept the bifurcation as a real feature in the HR diagram, several scenarios could, in principle, account for it. The first is contamination from foreground field stars. However, as mentioned, HC00 found the expected field star contribution to be only ∼5% down to the completeness limit of K∼17.5. whereas the apparent low luminosity population accounts for a much larger fraction ($\sim \frac{1}{3}$) of my sample. The second possibility is that there is contamination by a foreground population of M stars, however it does not originate from the field but from the surrounding OB association. The ONC (also known as Orion subgroup Id) is neighbored by three somewhat older subgroups of stars (Ia, Ib, & Ic; see Brown et al. 1994 for a detailed description of each) which are located at distances ranging from ∼360 to 400 pc and having ages (derived from high mass populations) from ∼2 to 11.5 Myr. The most likely subgroup which could contribute contamination to the survey data is subgroup Ic, which is located along the same line of sight as the ONC. However, its members are thought to be only ∼2 Myr old and therefore cannot account for the stars on the lower branch in the HR diagram unless their age estimate is in error. The only known part of the OB association which could be contributing ∼10 Myr old stars to the study is subgroup Ia, which is estimated to be ∼11.4 Myr.

While the known high mass population of the Ia subgroup does not extend spatially as far as the ONC, if there has been dynamical relaxation, it is possible that its lower mass members may occupy a more widespread area than the OB stars. Brown et al. (1994) found the initial mass function for the subgroups to be a single power law of the form $\xi(\log M) \propto M^{-1.7\pm0.2}$ based on the high mass population ($M > 4$ $M_\odot$). Since the lower mass members have not yet been identified or studied in detail, I extrapolate the high-mass IMF to determine the total number of stars in subgroup

Ia expected down to 0.02 $M_\odot$ and find there should be ∼3500 members. This number is an upper limit since I have not applied a Miller-Scalo turnover to the IMF but simply extended the power law form. The angular size of the Orion Ia subgroup as studied by Brown et al. (1994) corresponds to a linear size of ∼45 pc. From this information I calculate a relaxation time for the cluster

$$t_{relax} = n_{relax} \times t_{cross} = \frac{8 \ln N}{N} \times \frac{R}{\sigma}.$$

Assuming a gravitationally bound cluster and a velocity dispersion of σ ∼2 km s^{-1} consistent with the ONC (Jones & Walker, 1988), I find a crossing time for the Orion Ia cluster of ∼11 Myr and a relaxation time of ∼600 Myr. Clearly the cluster is not yet dynamically relaxed and it is unlikely that its low mass population would have spread significantly past its higher mass members. This calculation does not however, rule out the possibility that the lower mass population formed over a wider spatial area than the massive stars, given that primordial mass segregation has been suggested in other young clusters (Hillenbrand & Hartmann, 1998).

From the same IMF extrapolation I find the surface density of 0.5-0.02 $M_\odot$ objects in subgroup Ia to be ∼2.5 pc^{-2}. The areal extent corresponding to the angular size of our survey region (assuming a distance of 480 pc) is ∼0.5 pc^2. Assuming a constant surface density across this area, it is expected that <2 members of Orion Ia would be found in the current work. Even if I ignore previous age estimates, assume all three of the subgroups could be contributing to the observed lower branch of the HR diagram, and repeat the above calculation for subgroups Ib & Ic, I would expect to see < 10 stars total. Therefore, it is unlikely that the lower branch seen in the inner ONC HR diagram is purely due to contamination from surrounding populations. I cannot rule out that there may exist a foreground population of ∼10 Myr stars which is not associated with the ONC, but which was missed by the Brown et al. (1994) work due to its dirth of OB stars. However, the probability that this population would lie in exactly the same line of sight as the ONC is small.

Another possible cause of the older branch of the HR diagram is scattered light

from circumstellar disks and envelopes. Most of the objects in the lower branch of the HR diagram have $(J-H)$,$(H-K)$ near-infrared excesses consistent with their being young objects surrounded by circumstellar material which could result in their detection primarily in scattered light. If true, extinctions, and consequently luminosities for these objects would be underestimated, making them appear older than the bulk of the population. Similar arguments have been put forth by Luhman et al. (2003b) to explain low-lying stars on the HR diagram of IC 348. One uncertainty in this argument is that if scattered light is responsible for causing the apparently older population, it would have to be acting on the observations in such a way so as to create a dichotomy of object luminosities rather than a continuous distribution of stars at unusually faint magnitudes. This scenario could occur however, if the lower luminosities measured for this population are caused by a drop in observed light due to the objects being occulted by a disk. The relatively low luminosities of substellar objects would make such systems more difficult to detect and we may be observing the brighter end of a distribution of low mass scattered light sources. In support of this argument, one of these sources is coincident with an optically identified *Hubble Space Telescope* "proplyd" (which is known to be a photoevaporating circumstellar disk), and two with disks seen optically in silhouette only (Bally et al., 2000).

If the lower luminosity population in the inner ONC is real, rather than due to systematics in the data reduction/analysis or contamination from the surrounding older association, the question arises as to why it was not seen in previous surveys. The deepest optical photometric survey in this inner region is that by Prosser et al. (1994) which is reported complete to V≈20 mag and I≈19 mag, though no details are given on how these numbers were derived or how they might vary with position in the nebula. One can view the photometric data of H97, which is a combination of ground-based CCD photometry out to 15' from the cluster center and the Prosser et al. (1994) HST CCD photometry in the inner 3' or so, in terms of color-magnitude diagrams binned by radial distance from the cluster center. At all radial distances there are some stars which sit low in the color-magnitude diagram. However, it is only in radial bins beyond ∼7' that a substantial population (though still disproportionately small

compared to the current findings) of apparently 10 Myr old low mass (0.1-0.3 $M_\odot$) stars begins to appear, as might be expected if they are contaminants from the Orion Ic association. The inner radial bins do not display this population, though it should have been detected at masses larger than 0.15 $M_\odot$ *in the absence of extinction.* Notably the apparently 10 Myr old population in figure 6.1 does not lack extinction. Figure 6.2 shows a histogram of extinction for sources included in figure 6.1. The open histogram indicates all objects; the hatched and shaded histograms include only the 1 and 10 Myr old populations, respectively. I find all three populations to have similar, roughly constant distributions for $A_K \lesssim 0.6$ ($A_V \lesssim 10$) giving further evidence that the lower luminosity branch of the HR diagram is likely not a foreground population. Accounting for typical errors ($\sim$0.1 mag at K and $\sim$1.5 mag at V; see Slesnick et al. 2004) will not change my conclusions. For extinction values larger than $\sim$2 visual magnitudes the 0.15-0.5 $M_\odot$ stars at 10 Myr in figure 6.1 would have been missed by the optical Prosser et al. (1994) photometric survey but uncovered in later infrared surveys. Further, Walker et al. (2004) find from theoretical work a lower incidence of disk occultation for higher mass classical T Tauri stars ($\sim$20% of systems with disks) in comparison to lower mass substellar objects (up to $\sim$55% of systems with disks) due to smaller disk scale heights and less disk flaring. Therefore, if the low luminosity objects are a population of scattered light sources smaller numbers of them may be expected at higher masses.

6.1.2 The ONC's Low-Mass IMF

Currently, there are relatively few sets of pre-main-sequence (PMS) evolutionary models which extend into the substellar regime. The Lyon group (Baraffe et al. 1998 & Chabrier et al. 2000; hereafter BCAH98) calculations cover 0.001–1.2 $M_\odot$, but do not extend to the large radii of stars younger than 1 Myr. Thus, they must be applied to young low-mass star forming regions with caution. The other widely utilized set of low-mass PMS models are those by DM97. These models cover 0.017–3.0 $M_\odot$ over an age range of 7×10^4 yr to 100 Myr, and are therefore representative of even extremely

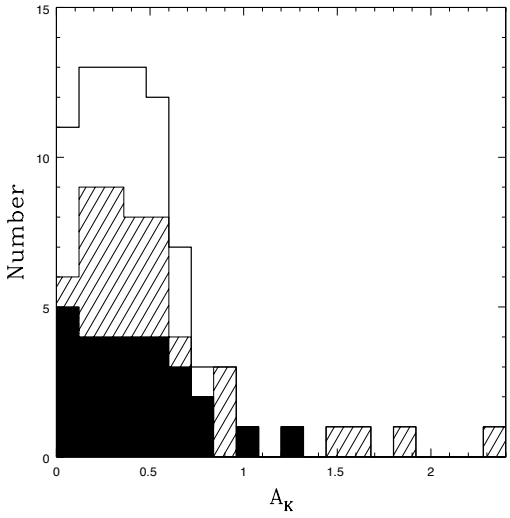

Figure 6.2 Histogram of extinction for sources included in figure 6.1. The open histogram indicates all objects; the hatched and shaded histograms include the two populations with apparent ages (as interpreted from the HR diagram) of ∼1 and ∼10 Myr old, respectively. Similar extinction distributions are found for all three populations.

young regions. A detailed analysis and comparison of the models is given by Hillenbrand & White (2004). For the purpose of the current work I use DM97 tracks and isochrones to determine masses and ages for stellar and substellar objects in our HR diagram.

Because the ONC is highly crowded and extremely nebulous, it is important to determine that the spectroscopic sample is representative of the population as a whole before using the sample to construct a cluster mass function. Figure 6.3 shows a histogram of completeness as a function of magnitude. Open and hatched histograms indicate the distribution of HC00 photometry and of sources for which I have spectral types, respectively. The hatched histogram includes not only sources for which I determined new spectral types, but also optically classified sources from the literature (H97 and references therein) which fall within the survey region and were determined to be of spectral type M0 or later. In combining the two data sets the goal is to assemble a statistically large sample of cool, spectroscopically confirmed ONC members down to extremely low masses (M ∼0.02 $M_{\odot}$) from which to create the IMF.

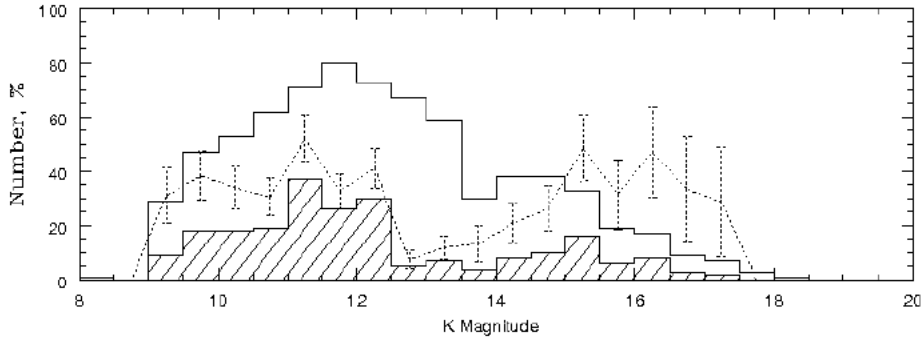

Figure 6.3 Histogram of HR diagram completeness as a function of magnitude. Open and hatched histograms indicate the distribution of all HC00 photometry and the subset for which we have spectral types, respectively. The dotted line in each panel indicates fractional completeness of the spectroscopic sample with $\sqrt{(N)}$ errorbars. Although the spectroscopic sample is ∼40% complete at bright and faint magnitudes, correction factors to the mass function are needed at intermediate magnitudes.

The dotted line in figure 6.3 indicates fractional completeness with $\sqrt{(N)}$ errorbars. I estimate that the stars included in figure 6.1 are ∼40% complete across the entire magnitude range with the exception of the $12.5 < K < 15$ bins. Undersampling at these intermediate magnitudes is caused by combing the sample of brighter, optically classified, mainly stellar objects with my sample of infrared-classified objects where the aim was to observe objects fainter than the substellar limit. Therefore, magnitude bins corresponding to masses near the hydrogen burning limit are underrepresented. I can correct for this deficiency by determining the masses which correspond to objects in the depleted magnitude bins. I then add stars to those mass bins according to the fractional completeness of the magnitude bins they came from, relative to the overall 40% completeness. I discuss both the corrected and corrected IMFs below.

Figure 6.1.2 shows the mass function for stars within the inner 5.'1 × 5.'1 of the ONC that have spectral types derived from either infrared or optical spectral data later than M0. The thick-lined open histogram, shown with $\sqrt{(N)}$ errorbars, includes all stars meeting this criteria which were not determined to have high surface gravity. In total, the IMF sample includes ∼200 stars and contains objects with masses as

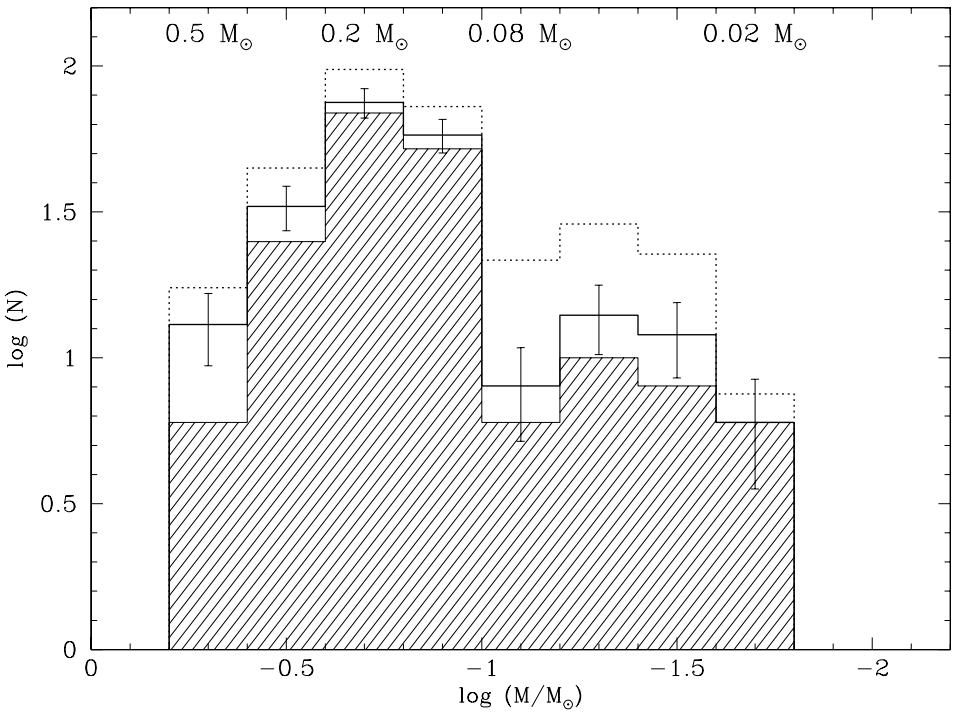

Figure 6.4 Mass function for all stars within the inner 5.'1 × 5.'1 of the ONC that have spectral types from the present work or the literature later than M0. Thick-lined open histogram shown with $\sqrt{N}$ errorbars indicates all stars; the dotted open histogram represents the same sample corrected for incomplete magnitude bins (figure 6.3). The hatched histogram indicates only stars younger than ∼5 Myr according to the HR diagram (figure 6.1).

high as ∼0.6 $M_\odot$ and as low as <0.02 $M_\odot$. Mass completeness (to the 40% level) extends from ∼0.4 $M_\odot$ (corresponding to an M0 star at 1 Myr; see figure 6.1) to the completeness limit of HC00, ∼0.03 $M_\odot$ for $A_V < 10$. The dotted open histogram indicates an IMF for the same sample, where I have corrected for the incomplete magnitude bins. The most substantial correction occurs right at the substellar limit as indicated above. The hatched histogram represents only those objects determined to be younger than 5 Myr from HR diagram analysis; thus, I remove any possible bias occurring by inclusion of the apparently older ∼10 Myr population which may or may not be a real part of the cluster. As can be seen, the apparently older stars constitute a relatively uniformly spaced population across the mass range I am exploring (see also figure 6.1), and including them in the IMF does not affect the interpretation.

The stellar-substellar IMF for the inner ONC in figure 6.1.2 peaks at ∼0.2 $M_\odot$ and falls across the hydrogen-burning limit into the brown dwarf regime. Using the observed IMF, I find ∼17% (39) of the objects in my sample to be substellar ($M <$ 0.08 $M_\odot$). Below ∼0.08 $M_\odot$ the mass distribution levels off through the completeness limit of ∼0.02 $M_\odot$. There may be a secondary peak at ∼0.05 $M_\odot$, but it is not statistically significant. Decreasing the bin size by 50% yields the same results, with the peak at 0.05 $M_\odot$ becoming even more pronounced. Increasing the binsize by 50% produces a steady decline into the substellar regime. The total mass inferred between 0.6 and 0.02 $M_\odot$ from these data is ∼41 $M_\odot$ which, corrected for the 40% completeness factor becomes ∼100 $M_\odot$. This value is a lower limit because, as I have already shown, the survey is not 40% complete at all magnitudes. I find an average mass of ∼0.18 $M_\odot$ corresponding to the peak in the data.

6.1.2.1 Comparison to Previous ONC IMF Determinations

The stellar/substellar IMF has been discussed in previous work on the ONC. A determination based on near-infrared photometric data was made by HC00 using H and K magnitudes and colors combined with star count data to constrain the IMF down to ∼0.03 $M_\odot$. They find a mass function for the inner regions of the ONC which rises to a peak around 0.15 $M_\odot$ and then declines across the hydrogen burning limit with

slope N($\log M$) $\propto M^{0.57}$. M02 transform the inner ONC's K-band luminosity function into an IMF and find a mass function which rises with decreasing mass to form a broad peak between 0.3 $M_\odot$ and the hydrogen-burning limit before turning over and falling off into the substellar regime. This decline is broken between 0.02 and 0.03 $M_\odot$ where the IMF may contain a secondary peak near the deuterium burning limit of ∼13 M_{Jup}. Luhman et al. (2000) combined near-infrared NICMOS photometry of the inner 140" × 140" of the ONC with limited ground-based spectroscopy of the brightest objects ($K < 12$) to determine a mass function which follows a power-law slope similar, but slightly steeper than the Salpeter value, until it turns over at ∼0.2 $M_\odot$ and declines steadily through the brown dwarf regime. H97 presents the most extensive spectroscopic survey of the ONC, combining optical spectral data with V and I-band photometry over a large area (∼2.5 pc^2) extending into the outer regions of the cluster. The IMF determination covers a large spectral range and appears to be rising from the high (50 $M_\odot$) to low (0.1 $M_\odot$) mass limits of that survey.

The peak in the IMF presented here, ∼0.2 $M_\odot$, matches remarkably well to those found from both the deep near-infrared imaging IMF studies (HC00 and M02) which cover similar survey areas, and the Luhman et al. (2000) study which covered only the very inner region of the cluster. My data also show a leveling off in the mass distribution through the substellar regime similar to that found by HC00. A significant secondary peak within the substellar regime has been claimed by M02. While I see some evidence for such a peak in my data, this result is not robust to within the errors. Furthermore, if real, I find the secondary peak to occur at a slightly higher mass than M02 (∼0.05 $M_\odot$ vs. ∼0.025 $M_\odot$). The primary difference between the observed IMF derived in the current work and those presented in previous studies of the substellar ONC population is the steepness of the primary peak and the sharpness of the fall-off at the hydrogen-burning limit (see for comparison figure 16 of M02). Most IMF determinations for this region exhibit a gradual turnover in the mass function around ∼0.2 $M_\odot$ until $\sim \frac{2}{3}$ the level of the primary peak is reached at which point the IMF levels off or forms a secondary peak. However, I find a sharp falloff beyond ∼0.1 $M_\odot$ to $\sim \frac{1}{2}$ the primary peak value.

6.1.2.2 Photometric vs. Spectroscopic Mass Functions

As mentioned in §6.1, spectroscopy is needed to study a cluster's IMF in more than a statistical sense. The fact that many of the fainter objects in my survey expected to be substellar based on their location in the K, $(H - K)$ diagram are in fact hotter, possibly older objects gives strong evidence in support of this statement. Independent knowledge of an individual star's age, extinction and infrared excess arising from the possible presence of a circumstellar disk is needed before definitive conclusions can be drawn about that object's mass. Despite the increasing numbers of brown dwarfs studied, both in the field and in clusters, details of their formation process remain sufficiently poorly understood that knowledge of near-infrared magnitudes and colors alone is not enough to accurately predict these characteristics for young low mass objects. Near-infrared magnitudes alone also cannot distinguish between cluster members and nonmembers, and field star contamination must be modeled rather than accounted for directly.

Previous studies of the ONC had spectroscopy available in general only for the stellar population, and relied on photometry alone to determine the mass function at substellar masses. This may have caused overestimates in the number of brown dwarfs for reasons discussed above. However, the more significant cause of the shallower peak in previous IMF determinations for the inner ONC as opposed to the sharply peaked IMF derived here is likely just the inherent nature of photometric vs. spectroscopic mass functions. Determining masses for stars in a sample from temperatures derived from spectral types necessarily discretizes the data. Conversely, photometric studies are by their nature continuous distributions, and deriving masses from magnitudes and colors or luminosity functions results in a smooth distribution of masses. I emphasize that while neither situation is ideal, mass functions derived for young objects from photometry alone represent only a statistically probable (given correct assumptions wer made) distribution of underlying masses. Spectroscopy is needed in order to derive cluster membership and masses for individual objects.

6.1.3 Summary of ONC Survey

I have identified for the first time a large sample of spectroscopically confirmed young brown dwarfs within the inner regions of the ONC, including five newly classified M9 objects. From this data I made an HR diagram and possibly discovered a previously unknown population of ∼10 Myr old low mass stars within the inner regions of the cluster. I examined this population in detail and determined that it is not an artifact arising from systematics in the spectral reduction/classification processes. I ruled out that this population consists primarily of "contaminants" from the surrounding OB1 association. If this population is real, I propose that it was not detected in previous works because of its intrinsic faintness, coupled with extinction effects. Another possible scenario is that these objects constitute a population of scattered light sources. If this hypothesis is correct, these objects provide indirect observational support for recent theoretical arguments indicating higher disk occultation fractions for young substellar objects in comparison to higher mass classical T Tauri stars (Walker et al., 2004).

From the HR diagram I used DM97 tracks and isochrones to infer a mass for each object and constructed the first spectroscopic substellar ($0.6 > M > 0.02$ $M_{\odot}$) IMF for the ONC. The mass function presented here peaks at ∼0.2 $M_{\odot}$ consistent with previous IMF determinations (M02; HC00; Luhman et al. 2000), however it drops off more sharply past ∼0.1 $M_{\odot}$ before roughly leveling off through the substellar regime.

6.2 Age/Mass Distributions of the Low Mass Population in USco

The details of my photometric/spectroscopic survey in USco were discussed extensively in chapters 2, 3 & 5. In this section I assess quantitatively the age and mass distribution of low mass association members. The discussion will proceed in a manner similar to that for the ONC (§6.1). I discuss first the age distribution as inferred from an HR diagram, and, subsequently, I derive a stellar/substellar mass function

for USco. In the next section (§6.3) I compare my results for both USco and the ONC to those in the literature for other young associations.

6.2.1 HR Diagram for Low Mass Members of USco

In figure 6.5 I present the HR diagram (originally shown as figure 5.2) for low mass PMS stars and brown dwarfs in USco. I have chosen to use DM97 tracks and isochrones for all analysis presented here for ease of comparison with results from the ONC survey. All derived quantities are given in table 6.1. Interpreting the ages literally, figure 6.5 reveals a population with a median age of ∼4.1 Myr and a continuous spread of ages over ∼10 Myr. While this result *may* be real, the continuous nature of the observed age distribution in USco is more likely to be produced from uncertainties in observed parameters than, for example, the bimodal distribution seen in my survey of the ONC (§6.1.1). Also suspicious is the fact that the surface gravity-sensitive spectral features do not show evidence for the same age spread. Figure 6.6 shows spectra of two stars with spectral type M5 identified in the USco survey. The top spectrum is of the 'youngest' M5 star observed spectroscopically at Palomar (SCH16054416-21550566), ∼2.6 Myr-old based on its location on the HR diagram (figure 6.5); the bottom spectrum is of a the 'oldest' M5 star observed at Palomar (SCH16162599-21122315), ∼14.4 Myr from the HR diagram. Recalling the discussion in §4.3, young stars less than a few megayears old exhibit systematically less Na I (λ8190 Å) absorption than do intermediate-age stars (∼5–10 Myr). Thus, if the derived ages from the HR diagram are correct, the spectrum of the 14.4 Myr-old star should have noticeably stronger Na I absorption. However, unlike the spectral sequence shown in figure 4.3 where the young and intermediate-age stars clearly show different surface-gravity spectral features, the spectra presented here are nearly identical (and have near-identical measured Na-8190 indices of 0.89 and 0.90). Based on analysis of spectral features, I classified these two stars as being roughly the same age. However, based on the differences in observed luminosity, interpreting the HR diagram literally, one would infer an age spread of >10 Myr between the two stars.

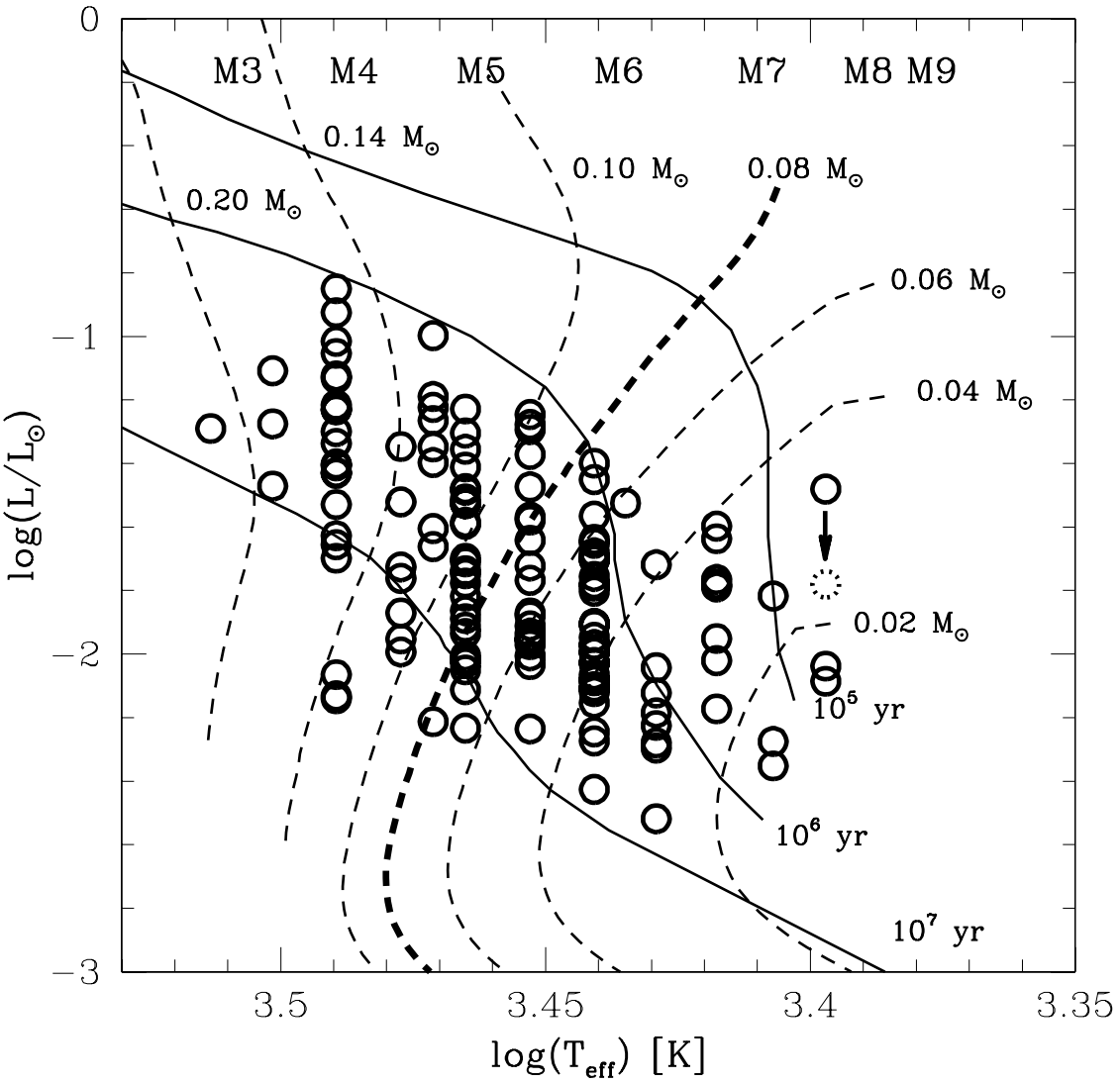

Figure 6.5 HR diagram for PMS objects discovered in my photometric/spectroscopic survey of the USco region. Literal interpretation of the HR diagram reveals a population with a median age of ∼4.1 Myr and an age spread from <1 Myr to >10 Myr.

Table 6.1. Derived quantities for new USco members

ID	$\log(T_{eff})$ [K]	$\log(L/L_\odot)$	$\log(age)$ [yr]	$M/M_\odot$
SCH15560497-21064632	3.41	-2.17	5.46	0.03
SCH15561978-24232936	3.47	-1.87	7.10	0.12
SCH15574757-24441236	3.49	-1.69	7.09	0.16
SCH15582337-21515908	3.47	-1.39	6.54	0.13
SCH15582566-18260865	3.44	-1.65	6.41	0.06
SCH15583162-24025411	3.47	-1.76	7.00	0.12
SCH15584812-21413426	3.45	-1.95	6.75	0.06
SCH15594802-22271650	3.40	-2.27	5.35	0.02
SCH15595868-18365205	3.45	-1.88	6.71	0.06
SCH16002669-20563190	3.47	-1.95	7.17	0.11
SCH16014156-21113855	3.49	-1.52	6.88	0.16
SCH16014768-24410152	3.46	-2.11	7.06	0.07
SCH16024143-22484204	3.45	-1.76	6.64	0.07
SCH16024576-23045102	3.46	-1.52	6.61	0.11
SCH16033470-18293060	3.46	-1.48	6.57	0.11
SCH16034029-23352386	3.49	-1.40	6.70	0.17
SCH16035651-23572517	3.47	-1.99	7.21	0.11
SCH16040453-23463795	3.49	-1.13	6.35	0.16
SCH16044303-23182620	3.42	-2.12	5.96	0.03
SCH16051829-17562092	3.49	-1.12	6.34	0.16
SCH16053077-22462016	3.44	-2.10	6.75	0.04
SCH16054416-21550566	3.46	-1.30	6.42	0.12
SCH16060391-20564497	3.41	-2.02	5.44	0.03
SCH16072239-20115852	3.45	-1.57	6.54	0.08
SCH16072640-21441727	3.44	-2.42	6.94	0.03
SCH16075565-24432714	3.45	-2.00	6.78	0.06
SCH16075850-20394890	3.44	-1.99	6.68	0.04
SCH16081081-22294303	3.46	-1.58	6.66	0.11
SCH16083646-24453053	3.50	-1.10	6.41	0.18
SCH16083658-18024994	3.42	-1.71	5.64	0.05
SCH16084058-22255726	3.49	-2.14	7.60	0.13
SCH16084170-18561077	3.44	-1.45	6.09	0.07
SCH16085870-24493641	3.49	-1.40	6.71	0.17
SCH16090451-22245259	3.41	-1.78	5.39	0.04
SCH16090511-24262843	3.49	-1.21	6.45	0.16
SCH16090771-23395430	3.46	-1.35	6.46	0.12
SCH16090883-22174699	3.46	-1.71	6.76	0.10

Table 6.1 (cont'd)

ID	$\log(T_{eff})$ [K]	$\log(L/L_\odot)$	$\log(age)$ [yr]	$M/M_\odot$
SCH16091837-20073523	3.40	-1.81	5.01	0.02
SCH16092137-21393452	3.45	-1.37	6.39	0.10
SCH16093018-20595409	3.44	-2.15	6.77	0.04
SCH16093707-20525337	3.47	-1.66	6.81	0.12
SCH16095217-21362826	3.41	-1.63	5.36	0.04
SCH16095307-19481704	3.44	-1.68	6.43	0.06
SCH16095695-22120300	3.45	-2.03	6.80	0.06
SCH16095991-21554293	3.42	-2.27	6.16	0.03
SCH16100129-21522466	3.45	-1.64	6.57	0.08
SCH16100541-19193636	3.44	-2.10	6.74	0.04
SCH16100751-18105666	3.44	-1.69	6.44	0.06
SCH16101190-21015540	3.45	-1.91	6.73	0.06
SCH16102990-24035024	3.47	-1.72	6.96	0.13
SCH16103525-20291714	3.46	-1.59	6.66	0.11
SCH16103876-18292353	3.44	-1.99	6.68	0.04
SCH16104635-18405996	3.47	-1.34	6.53	0.14
SCH16105500-21261422	3.44	-1.63	6.40	0.06
SCH16105727-23595416	3.49	-1.62	7.01	0.16
SCH16110144-19244914	3.46	-1.86	6.88	0.09
SCH16110739-22285027	3.43	-1.52	5.75	0.06
SCH16111711-22171749	3.40	-2.35	5.38	0.02
SCH16112629-23400611	3.45	-1.93	6.74	0.06
SCH16112959-19002921	3.44	-1.90	6.61	0.05
SCH16114735-22420649	3.46	-1.88	6.90	0.09
SCH16115737-22150691	3.46	-2.02	7.00	0.08
SCH16121044-19322708	3.46	-1.41	6.51	0.12
SCH16121188-20472698	3.42	-2.04	5.87	0.03
SCH16122764-24064850	3.41	-1.76	5.39	0.04
SCH16123459-24583447	3.47	-1.34	6.49	0.13
SCH16123758-23492340	3.44	-2.11	6.75	0.04
SCH16124506-23053043	3.45	-1.95	6.75	0.06
SCH16124692-23384086	3.44	-2.02	6.70	0.04
SCH16125723-24280145	3.49	-1.65	7.04	0.16
SCH16130306-19293234	3.45	-1.87	6.70	0.06
SCH16130764-17035233	3.45	-1.97	6.76	0.06
SCH16131212-23050329	3.42	-2.22	6.09	0.03
SCH16131857-15293460	3.47	-1.18	6.34	0.13

Table 6.1 (cont'd)

ID	$\log(T_{eff})$ [K]	$\log(L/L_\odot)$	$\log(age)$ [yr]	$M/M_\odot$
SCH16132576-17373542	3.49	-1.43	6.74	0.17
SCH16132809-19245288	3.44	-1.70	6.45	0.06
SCH16141351-22445788	3.49	-1.42	6.74	0.17
SCH16141484-24270844	3.41	-1.59	5.35	0.04
SCH16141974-24284053	3.44	-2.06	6.72	0.04
SCH16143286-22421358	3.42	-2.29	6.18	0.03
SCH16150524-24593542	3.46	-1.52	6.61	0.11
SCH16151115-24201556	3.44	-2.24	6.82	0.04
SCH16151360-23042637	3.42	-2.51	6.89	0.03
SCH16153915-19170073	3.47	-0.99	6.08	0.13
SCH16155508-24443677	3.44	-1.90	6.61	0.05
SCH16162396-24083016	3.46	-1.77	6.81	0.09
SCH16162599-21122315	3.46	-2.23	7.16	0.07
SCH16163504-20575551	3.45	-1.47	6.48	0.09
SCH16164538-23334143	3.46	-2.05	7.01	0.08
SCH16165160-20485398	3.49	-1.29	6.56	0.16
SCH16171901-21371312	3.45	-1.94	6.75	0.06
SCH16172504-23503799	3.46	-1.93	6.93	0.08
SCH16173105-20504715	3.41	-1.78	5.39	0.04
SCH16173238-20403653	3.44	-2.27	6.84	0.04
SCH16173788-21191618	3.49	-1.33	6.61	0.16
SCH16174368-21115536	3.49	-2.13	7.59	0.13
SCH16174540-23533618	3.44	-2.08	6.73	0.04
SCH16181201-24133263	3.46	-1.47	6.57	0.11
SCH16181567-23470847	3.45	-1.24	6.26	0.10
SCH16181601-24372688	3.49	-1.05	6.26	0.16
SCH16181906-20284815	3.47	-1.22	6.37	0.13
SCH16182501-23381068	3.46	-1.81	6.85	0.09
SCH16183144-24195229	3.42	-2.18	6.04	0.03
SCH16183620-24253332	3.49	-1.23	6.47	0.16
SCH16185038-24243205	3.46	-1.91	6.92	0.08
SCH16190473-23075283	3.45	-1.72	6.62	0.07
SCH16191521-24172429	3.49	-1.22	6.47	0.16
SCH16192994-24255414	3.49	-0.85	6.05	0.15
SCH16193976-21453527	3.44	-1.80	6.53	0.05
SCH16200756-23591522	3.44	-1.75	6.49	0.05
SCH16201318-24250155	3.49	-2.06	7.52	0.14

Table 6.1 (cont'd)

ID	$\log(T_{eff})$ [K]	$\log(L/L_\odot)$	$\log(age)$ [yr]	$M/M_\odot$
SCH16202127-21202923	3.44	-1.90	6.61	0.05
SCH16202523-23160347	3.45	-2.23	6.94	0.05
SCH16211564-24361173	3.50	-1.47	6.93	0.19
SCH16211922-24255250	3.49	-1.01	6.22	0.16
SCH16212490-24261446	3.50	-1.27	6.64	0.19
SCH16213591-23550341	3.44	-2.02	6.70	0.04
SCH16221577-23134936	3.44	-2.08	6.73	0.04
SCH16222156-22173094	3.46	-2.00	6.98	0.08
SCH16224384-19510575	3.39	-1.48	7.15	0.04
SCH16235158-23172740	3.39	-2.03	5.31	0.02
SCH16235474-24383211	3.44	-1.70	6.45	0.06
SCH16252862-16585055	3.39	-2.08	5.33	0.02
SCH16252968-22145448	3.46	-1.73	6.78	0.10
SCH16253671-22242887	3.41	-1.95	5.42	0.03
SCH16254319-22300300	3.46	-1.74	6.79	0.10
SCH16255064-21554577	3.47	-2.21	7.28	0.08
SCH16260630-23340375	3.45	-1.56	6.53	0.08
SCH16263026-23365552	3.44	-1.77	6.51	0.05
SCH16265619-22135224	3.44	-1.94	6.64	0.05
SCH16270940-21484591	3.47	-1.52	6.73	0.14
SCH16274801-24571371	3.46	-1.69	6.75	0.10
SCH16281810-24283619	3.44	-1.39	5.95	0.08
SCH16284706-24281413	3.44	-1.78	6.51	0.05
SCH16292211-17420937	3.47	-1.60	6.75	0.12
SCH16293625-24565325	3.44	-1.97	6.66	0.05
SCH16293664-17084094	3.47	-1.26	6.41	0.13
SCH16293934-16145647	3.51	-1.29	6.79	0.22
SCH16294877-21370914	3.46	-1.51	6.60	0.11
SCH16302675-23590905	3.44	-1.56	6.34	0.07
SCH16303392-24280657	3.49	-0.92	6.13	0.15
SCH16305349-24245439	3.45	-1.27	6.31	0.10
SCH16310241-24084335	3.46	-1.22	6.35	0.12
SCH16324224-23165644	3.45	-1.29	6.33	0.10
SCH16324726-20593771	3.44	-1.97	6.66	0.04

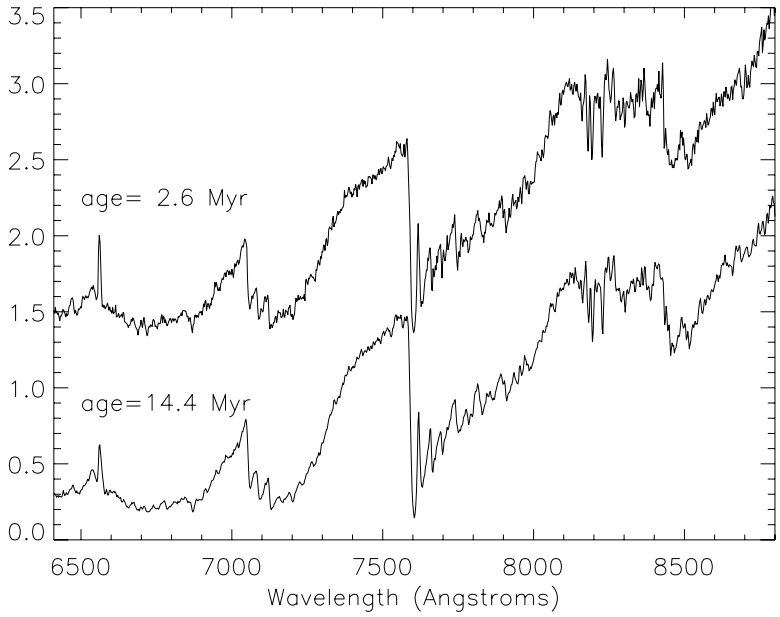

Figure 6.6 Spectra of two stars with spectral type M5 found in the USco survey. The top spectrum is of the 'youngest' (based on analysis of the HR diagram) M5 star observed spectroscopically at Palomar, ∼2.6 Myr-old; the bottom spectrum is of a the 'oldest' (based on analysis of the HR diagram) M5 star observed at Palomar, ∼14.4 Myr. These stars have near-identical spectra, and, based on analysis of the strength of the surface gravity sensitive Na I line (8190 Å), appear to be the same age. However, based on the differences in observed luminosity, interpreting the HR diagram literally, one would infer an age spread of >10 Myr between the two stars.

Due to the discrepancy between stellar ages derived from surface gravity analysis and HR diagram analysis, I sought to determine the statistical significance of the apparent spread in ages from the HR diagram. To assess this value quantitatively, I used Monte Carlo techniques to simulate a coeval 5 Myr-old population of stars at the mean distance (145 pc) of USco. The stars in my sample were placed onto the HR diagram in figure 6.5 based on observed J magnitudes, $J-H$ colors, and spectral types (see chapter 5). Once a star is placed onto the HR diagram from effective temperature and luminosity, age and mass are inferred using a set of theoretical isochrones and mass tracks. Thus, uncertainties in measured photometry or spectral types are propagated into uncertainties in mass and age. Variations in distance and

binarity can cause additional uncertainty in luminosity, and hence, quantities derived from the HR diagram.

I sought to explore if I could recreate the apparent age spread in the HR diagram using only known uncertainties. To accomplish this goal, I generated a population of 5 Myr-old stars and brown dwarfs at a distance of 145 pc. The input spectral type distribution was selected to mirror that of my observed distribution of stars, in that for every observed star of a given spectral type, 1000 stars of that starting spectral type were simulated. From my starting population I varied the J- and H-band magnitudes by adding random offsets drawn from a Gaussian distribution with a 1-sigma deviation of 0.025 mag, corresponding to the average uncertainty in the 2MASS photometry for observed stars. To mimic the magnitude-limited data sample, I did not allow any star to be simulated below the photometric survey limits (J=16 and H=15.5). Similarly, I added a random offset to the assumed spectral type selected from a Gaussian distribution with 1-sigma errors of 0.5 spectral subtypes corresponding to the qualitative error of the optical spectral type determinations. Using the new spectral type, for each simulated star I re-derived the expected effective temperature, bolometric correction and intrinsic $J-H$ color using the methods described in Slesnick et al. (2004).

The maximum distance spread (derived from secular parallax measurements) among members of the association with Hipparcos measurements is predicted to be 50 pc (Preibisch et al. 2002; de Bruijne 1999). In the simulation I assumed a uniform spatial distribution over a box of this depth centered at 145 pc. I assumed a 33% binary fraction for stars across all simulated spectral types (M3–M8), as derived by Kraus et al. (2005) from high resolution imaging observations. This study also finds all observed binaries to have near equal masses ($m_{secondary}/m_{primary} \gtrsim 0.6$) consistent with results for low mass stars in the field and in open clusters. For the purpose of this exercise, I made the assumption that all binaries were composed of two equal mass stars. This is assumption is somewhat conservative in that it will produce the largest possible dispersion in luminosity.

Figure 6.7 shows the same information as figure 6.5 with the addition of blue

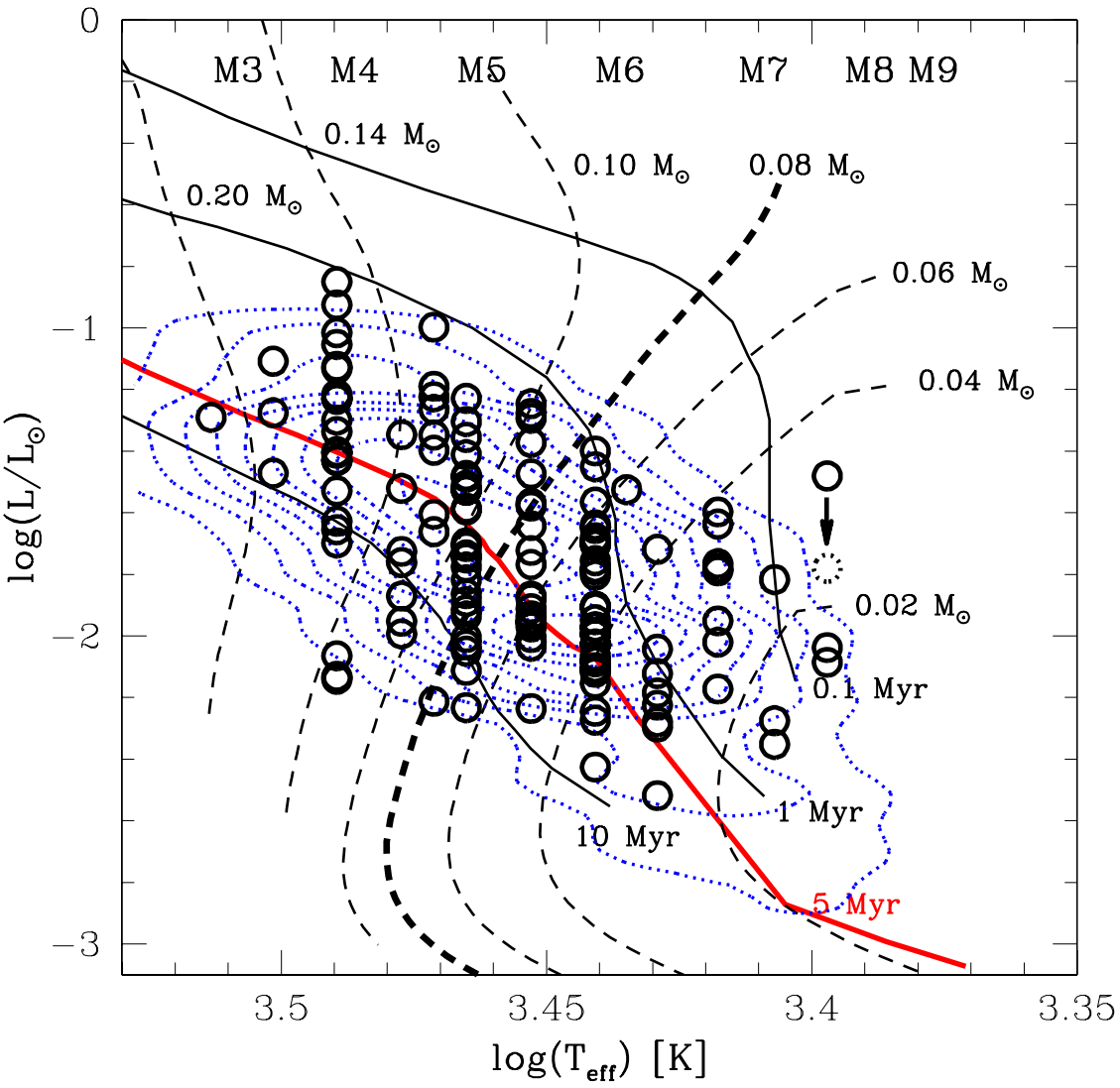

Figure 6.7 HR diagram for low mass members of USco. Blue contours are results from a numerical Monte Carlo simulation aimed at modeling the expected observed age spread given a coeval 5 Myr-old population with known observable uncertainties (see text for more details). Contours are shown at 90%–10% of the peak level.

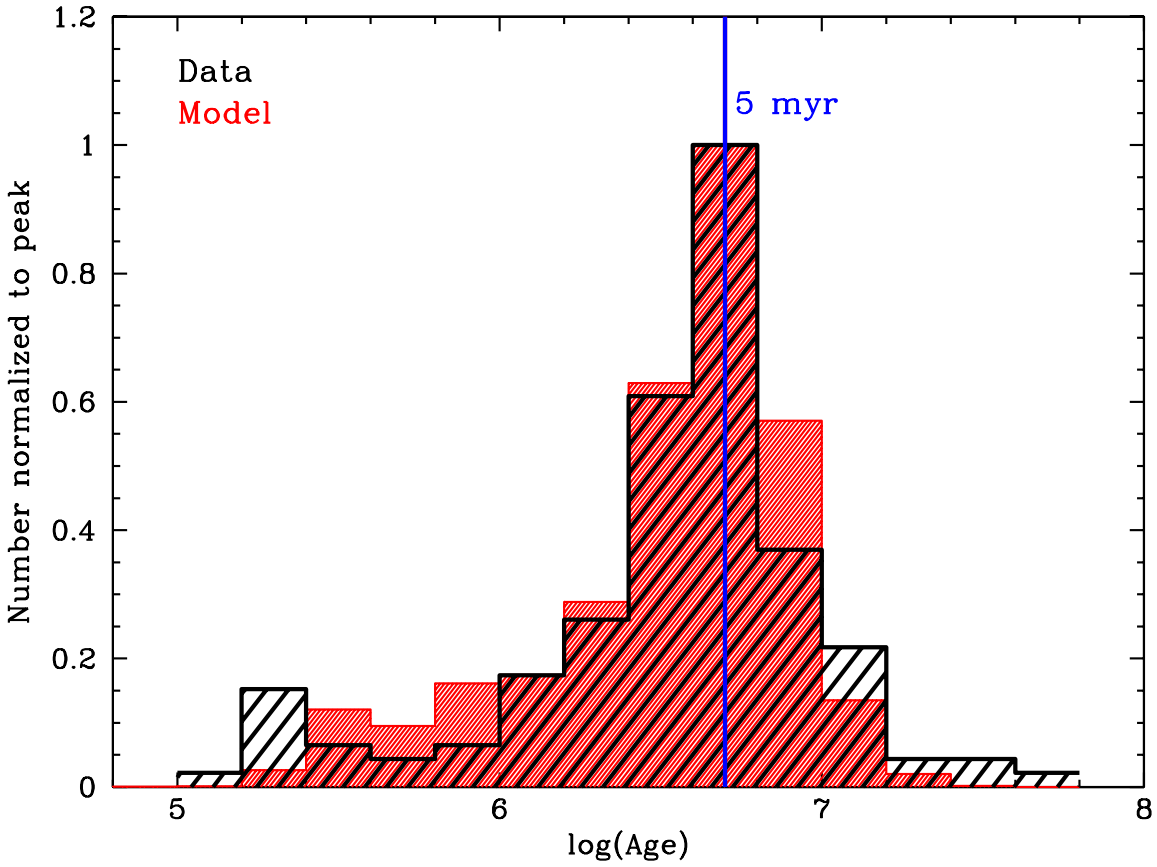

Figure 6.8 Red shaded histogram shows the age distribution derived from the Monte Carlo simulation, overplotted with a histogram of ages for the data (black hatched histogram). Both histograms have been normalized to one at the peak for comparison, and all stars having $\log(T_{eff})$ <3.4 (beyond which interpolation of the isochrones becomes unreliable) have been excluded from both the data and the model results. The widths of the distributions are remarkably similar, given the simplistic nature of the Monte Carlo simulation.

contours representing the model output. Contours are shown at 90%–10% of the peak. As can be seen, much of the age spread in the HR diagram *could* be caused by uncertainties in the data rather than by an intrinsic spread in ages. I examine this result further in figure 6.8. The red shaded histogram shows the age distribution derived from the Monte Carlo simulation, overplotted with a histogram of ages for the data (black hatched histogram). Both histograms have been normalized to one at the peak for comparison, and all stars with $\log(T_{eff})$ <3.4 (beyond which interpolation of the isochrones becomes unreliable) have been excluded from both the data and the model results. The widths of the distributions are remarkably similar, given the simplistic nature of the Monte Carlo simulation. For the simulated association I find a median apparent age of $\log(age)$=6.62±0.41 whereas for the data (not including the 3 M8 stars) I find a median age of $\log(age)$=6.62±0.47. While all input parameters were realistic assumptions, I did not vary the expected photometric uncertainty as a function of magnitude, and I assumed that the population of USco consists of a box of stars with a constant stellar density. Because the output from this simple simulation produced a reasonable match to the data, I did not find a need to try a more complicated set of initial assumptions. A KS test yields a 70% probability that the distributions from the model output and the data could be drawn from the same population. Thus, given the uncertainties, the data are consistent with most stars in USco forming via a single burst ∼5 Myr ago.

This result is somewhat surprising given the large extent of the association (∼35 pc across). Assuming a sound speed of c_S=0.2 km/s consistent with a T=10 K molecular cloud, and assuming the stars formed close to where they are observed today, the sound crossing time for the parental molecular cloud is ∼85 Myr. Thus, one end of the cloud could not have 'communicated' to the other in time to create a simultaneous burst of star formation. This result does not, however, rule out the possibility that star formation happened simultaneously throughout the extent of the cloud because every part independently reach the threshold for star formation at the same time. Another scenario is that the stars formed much closer together and have since spread to their current positions. However, this possibility can be ruled out from

simple arguments. The velocity dispersion of the Hipparcos members is ∼1.3 km/s (de Bruijne, 1999). Thus, in 5 Myr the furthest an association member is expected to travel is ∼6.5 pc, less than half the radius of the current association.

This discrepancy between the small observed age spread for USco's stellar members and the large spatial extent of the population has been noted previously in the literature. To explain the disparity, Preibisch & Zinnecker (1999) (and later Preibisch & Zinnecker 2007) proposed a scenario in which star formation in USco was triggered by an external event in the form of a supernova explosion in the neighboring Upper Centaurus-Lupus association (∼70 pc away and ∼17 Myr-old). They argue based on the structure and kinematics of large H I loops surrounding Sco Cen, that such an event is evidenced to have occurred ∼12 Myr ago. If true, the explosion would have driven a shock wave which would have reached USco about ∼5 Myr ago, consistent with the inferred age of USco's stellar population. My results imply a similar small age spread with an association age ∼5 Myr and large spatial extent (see §5.3.4) for USco's lowest mass stars and substellar members. While this conclusion in no way proves the Preibisch & Zinnecker (1999) hypothesis true, it does give support to its plausibility and extend its validity to even the lowest mass association members.

In figure 6.8 the model and data differ from each other most significantly at the distribution tails. Specifically, the data are composed of more very young and very old stars than expected. Deriving ages from the DM97 isochrones, I observed 8 stars with age <2.5×10^5 yr (log(age)<5.4) and 15 stars with age >10 Myr (log(age)>7). If I scale down the results from the model to match the total number of stars present in my dataset (142 stars with $\log(T_{eff}) > 3.4$), the predicted number of observed stars in these age ranges is 1.2 and 6.9 for the young and old tails, respectively. Assuming Poisson statistics, the probability that out of the 142 stars I would have observed 8 or more stars younger than 2.5×10^5 yr is

$$P = \sum_{k=0}^{8} \frac{e^{-1.2} 1.2^k}{k!} = 0.004\%.$$

Using a similar equation, the probability that I would have observed 15 or more stars

older than 10 Myr is 0.5%.

There is no systematic spatial correlation between stars within the young and old age bins (see table 6.1). The young tail is, however, comprised only of the lowest mass, latest spectral type stars. This result is suspicious of an observational bias in that for a magnitude limited sample, I expect to preferentially observe the brightest (i.e., youngest) stars at low masses. To test this possibility, I ran a second version of the Monte Carlo simulation but requiring all simulated stars to be brighter than the faintest spectroscopic target confirmed to be a USco member ($J \sim$15 mag). However, this constraint yielded little change in the overall shape of the modeled age distribution and did not recover any of the stars with $age < 2.5 \times 10^5$ yr. Thus, *assuming the absolute validity of the model isochrones*, and assuming I made a correct assumption by using Poisson statistics, the group of young stars does appear to be real and may be evidence for recent star formation in USco. It should be noted, however, that the isochrones younger than $\sim$5 Myr begin to decrease sharply in luminosity at temperatures less than $\log(T_{eff}) \sim 3.45$ (see figure 6.7), while the data do not. Because my simulation input assumed a constant age of 5 Myr, the resulting distribution follows the 5 Myr isochrone, not the younger ones. Thus, the young group of stars may be illustrative of a systematic problem with the youngest isochrones at the lowest masses (i.e., perhaps the turnover in luminosity beyond $\log(T_{eff}) \sim 3.45$ is not accurate) rather than a real feature of the USco population.

Similar arguments could be made for the older group of stars. The old tail is comprised only of the earliest spectral type stars (spectral type $\lesssim$M5) where the DM97 isochrones at ages >5 Myr begin to get systematically closer together than they are for cooler stars. This fact leads to systematically larger numbers of hotter (<M5) stars to have derived ages $\gtrsim$10 Myr compared to later spectral types. A detailed test of the theoretical models is beyond the scope of this work. At this time I simply reiterate the point that theoretical isochrones for low mass PMS stars and young brown dwarfs are still not well understood, and results derived from these models must be used as a guideline for analysis only, rather than as literal truth.

6.2.2 USco's Low-Mass IMF

In this section I use the model tracks of DM97 to derive the first spectroscopic mass function for stars and brown dwarfs in USco less massive than ∼0.1 $M_\odot$. The study by Preibisch et al. (2002) derived an IMF for the *stellar* population in the association by combining the 166 spectroscopically confirmed low mass members (M∼0.8–0.1 $M_\odot$) discovered via their 2dF survey with the 120 known Hipparcos members (constituting a complete sample of members more massive than ∼1 $M_\odot$) and 84 X-ray selected members (M ∼0.8–2 $M_\odot$; Preibisch & Zinnecker 1999). The resultant mass function yielded a 3-segment power law function that was consistent with other recent field star and cluster IMF determinations above ∼2 $M_\odot$, but with a 2σ excess of stars at lower masses.

The only previous survey that has attempted to derive an IMF for USco's substellar members is the photometric study by Lodieu et al. (2007). This work observed ∼6.5 deg^2 of USco at $ZYJHK$-bands as part of the UKIRT Infrared Deep Sky Survey (UKIDSS) Galactic Cluster Survey. From these data, they used the J-band luminosity function to derive a *photometric* IMF in USco from 0.3–0.007 $M_\odot$. They derived a mass function that was significantly flatter ($dN/dM \propto M^{-0.3\pm0.1}$) than the IMF derived by Preibisch et al. (2002) for similar mass ranges ($dN/dM \propto M^{-0.9\pm0.2}$ for $0.1 \leq M/M_\odot < 0.6$). However, as noted in §6.1.2.2, great care must be taken when interpreting photometrically derived IMFs as they are based on incomplete knowledge of individual stellar ages, photometric excesses, and extinctions, and they cannot directly (only statistically) correct for field star contamination.

However, as was shown in §6.2.1, deriving quantities from an HR diagram has its own set of uncertainties. I have already shown that known uncertainties in observable magnitudes and spectral types can produce an apparent age spread of ∼10 Myr. I now wish to explore variation in the apparent mass distribution derived for stars in my sample. The top panel of figure 6.9 shows the apparent mass function derived for the 145 spectroscopically confirmed members shown in the HR diagram (figure 6.5). The bottom panel shows the derived mass function for a theoretical coeval population

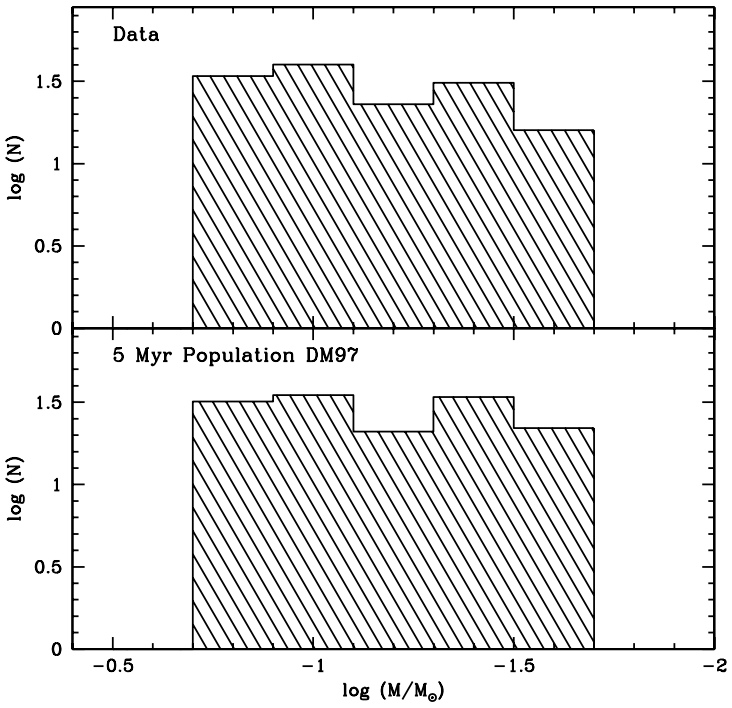

Figure 6.9 Top panel shows the apparent mass function derived for the 145 spectroscopically confirmed members shown on figure 6.5. Bottom panel shows the apparent mass function for a theoretical population of 145 stars with a uniform age of 5 Myr and a spectral type distribution consistent with that for the observed stars.

of 145 stars at an age of ∼5 Myr. To derive this IMF, I have assumed a spectral type distribution consistent with that for my observed population, and assigned each star the mass that it would have at that spectral type if it were 5 Myr-old. In both panels, data have been binned in steps of $\log(M)$=0.2. I have examined the difference between the two mass distributions using a KS test and find that the mass distributions derived from the real data and the theoretical 5 Myr-old population are statistically consistent with each other (probability=12%). Because the mass tracks are close to vertical for low mass stars (see figure 6.5), the dominant source of uncertainty in derived masses will come from uncertainties in temperature stemming from uncertainties in spectral type. My spectral type uncertainties are ±0.5 subtypes which is not enough to shift the derived mass by $\log(M)$=0.2 at any spectral type and the derived histograms will not change significantly. Presuming I am equally likely to misclassify a star 0.5 subtypes too early as I am to misclassify it 0.5 substypes too late, the mass distribution itself should not change significantly either. Thus, I conclude that the mass distribution derived from the HR diagram is more robust to observable uncertainties than I found the age distribution to be.

In figure 6.10 I show again the IMF derived from my spectroscopic survey of low mass stars and brown dwarfs, covering the mass range M ∼0.2–0.02 $M_{\odot}$. I have thus far observed spectroscopically only ∼15% of the photometric PMS candidates in the USco region. Therefore, before constructing a mass function, it is necessary to determine that the spectroscopic sample presented here is representative of the USco low mass population as a whole. I use a method similar to that employed in the ONC to determine the completeness of my sample. In the ONC, I binned the photometric and spectroscopic surveys as a function of magnitude and used this information to determine the relative completeness of the spectroscopic sample. This method was employed because at these masses in an $H, H-K$ diagram, the isochrones are almost vertical (see figure 1 of Slesnick et al. 2004). However, for the optical Quest-2 survey, I selected as candidate PMS stars all stars red-ward of the 1% data contour (see figure 3.3), and the selection cut was made along lines that depended on both r magnitude and $r-i$ color. Thus, to correct for incompleteness in the optical

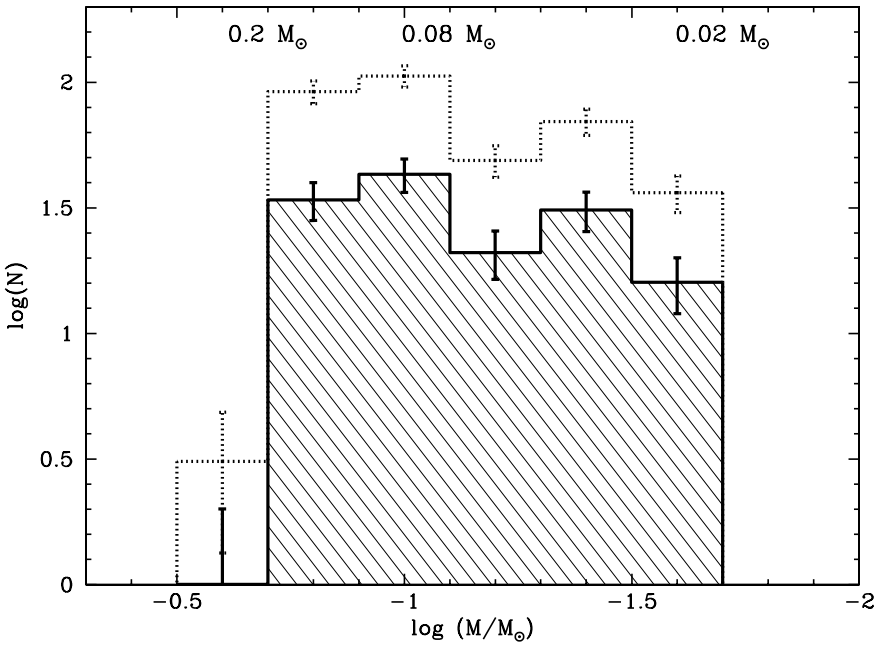

Figure 6.10 Mass function for all spectroscopically confirmed members presented in chapter 5. Thick-lined hatched histogram indicates all stars; the dotted open histogram represents the same sample corrected for incomplete selection bins (§6.2.2).

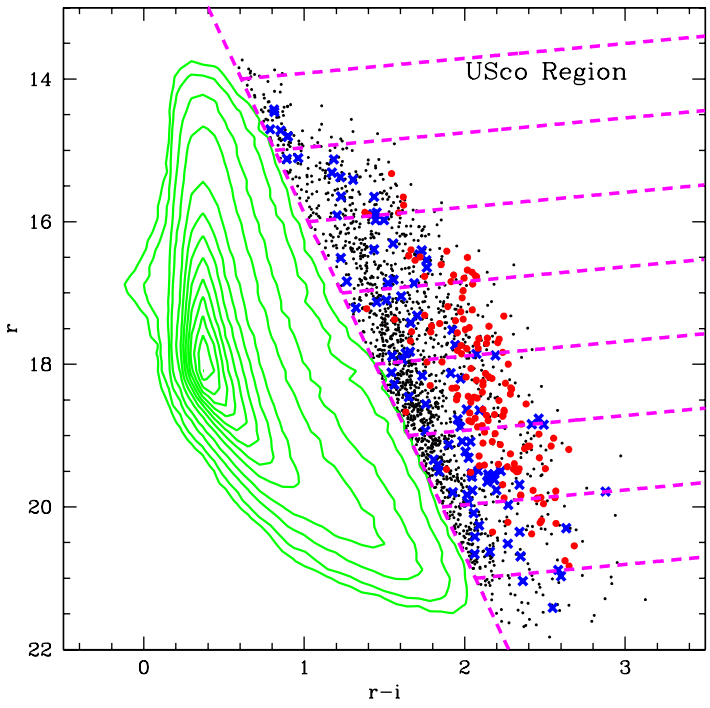

Figure 6.11 Optical Quest-2 $r, r-i$ CMD for the USco survey region. Photometric candidates (as defined in chapter 3) are shown as discrete points. Spectroscopic candidates are shown as large colored symbols: red circles are stars determined to be USco members based on spectral features. Blue X's are stars determined to be field dwarfs. The dashed, nearly vertical magenta line represents the 1% contour used in candidate selection (§3.1). Near horizontal magenta lines (perpendicular to the 1% contour line) delineate bins used to compute the spectroscopic completeness fraction.

photometric survey I computed the number of stars in bins perpendicular to the line of selection as shown in figure 6.11. The resulting histograms are shown in figure 6.12 for all photometric candidates (top panel) and for those observed spectroscopically (middle panel). Bin centers correspond to the middle of the bin in r magnitude at the selection line. The bottom panel in figure 6.12 shows the percentage of stars observed spectroscopically with $\sqrt{(N)}$ errorbars. As can be seen, priority in spectroscopic observations was given to faint stars, but with numbers of observed stars falling off considerably for stars fainter than r $\sim$19.5 which could be observed only under the best seeing conditions. The spectroscopic survey completeness peaks at $\sim$20%, and I followed the same method used in the ONC to correct all bins to this completeness level. The dotted histogram in figure 6.10 shows the IMF corrected to a uniform 20% completeness across all $r, r-i$ bins shown in figures 6.11 & 6.12. The derived mass function for USco is relatively flat across the mass range sampled and does not exhibit the sharp drop off at the substellar limit as seen for stars in the ONC.

In order to increase my sample size (improve statistics) and extend it to higher masses, I combined masses derived for my sample with those for stars from the Preibisch et al. (2002) survey. I chose to use this sample because 1) it constitutes the largest sample of spectroscopically confirmed low mass stellar members, and 2) candidates were selected from an $I, R-I$ CMD in an analogous manner to the methods employed to select my sample (chapter 3.1), and thus provide a complementary dataset. I specifically chose not to include the higher mass X-ray selected sources (Preibisch & Zinnecker, 1999) due to the large difference in selection techniques. To provide the most analogous samples possible, I re-derived masses for the 166 stars in the Preibisch et al. (2002) survey using the DM97 tracks and the same interpolation program used to generate masses for the sample of stars presented here. In combining samples from multiple sources one must be careful to account for relative completeness. Preibisch et al. (2002) estimate spectroscopic completeness levels of 87% for stars with $0.2 < M/M_{\odot} < 0.8$ and 67% for stars with mass <0.2 $M_{\odot}$, whereas, my corrected survey is only 20% complete across all sampled mass bins. The two surveys also cover very different areas. Preibisch et al. (2002) looked at 9 deg^2 whereas

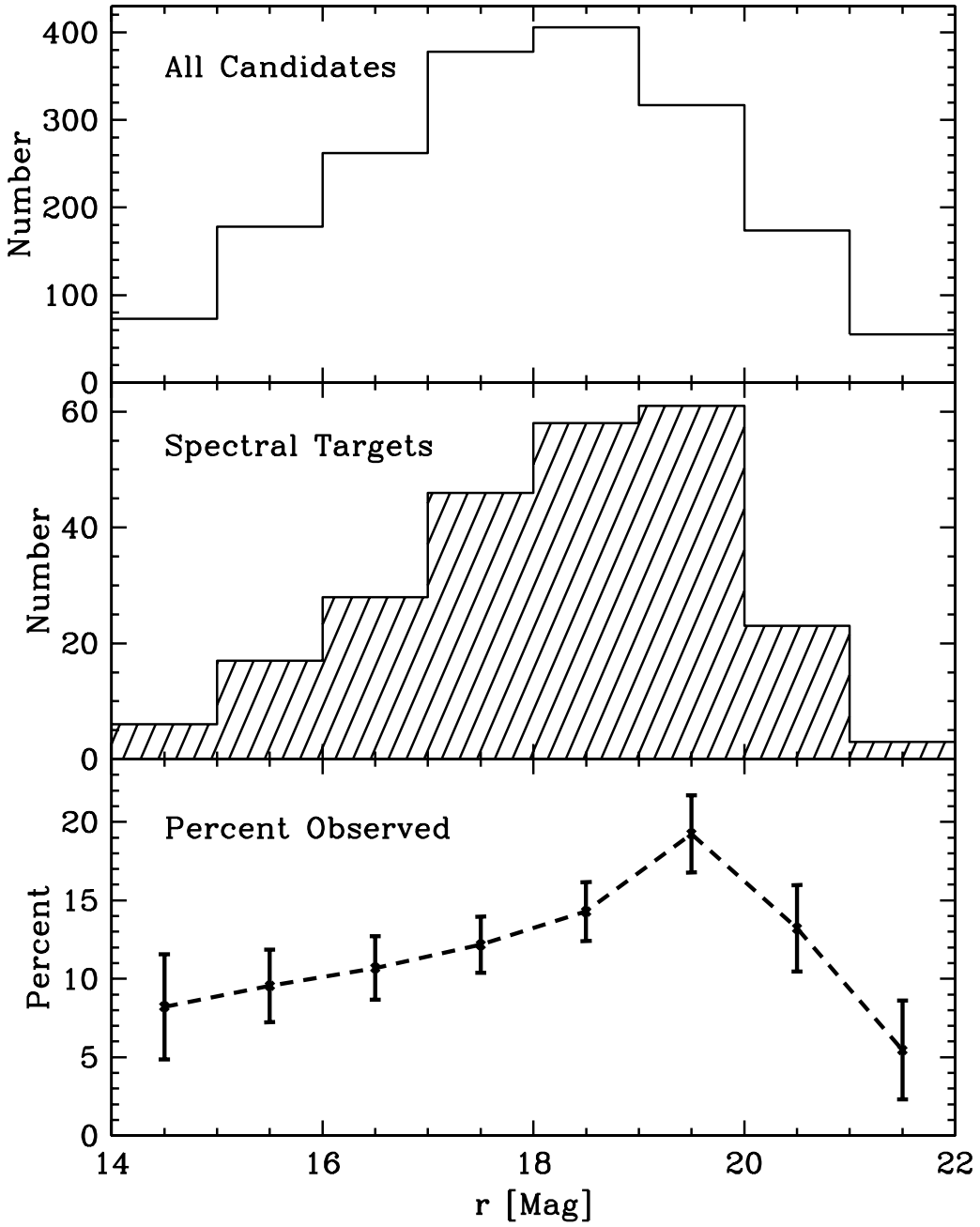

Figure 6.12 Histogram of optical CMD completeness as a function of r magnitude. Bin centers correspond to r magnitudes at the 1% contour line in figure 6.11. The top panel shows data for all photometric candidates and the middle panel shows data for all targets observed spectroscopically. As can be seen, faint targets were preferentially observed before brighter ones. The bottom panel shows the percent completeness with $\sqrt{(N)}$ errorbars. This quantity peaks at 20% near r=19.5 mag.

the Quest-2 survey looked at ∼150 deg^2. However, as mentioned in chapter 2, the Quest-2 survey coverage within this area is not complete due to several failed CCDs, gaps between the CCDs, and incomplete $r-i$ color coverage. Taking all of these factors into account, the total usable Quest-2 survey area is ∼100 deg^2. The number of stars in the Preibisch et al. (2002) survey were thus multiplied by either (100 deg^2/9 deg^2)×(20% complete/87% complete) for stars with $0.2 < M/M_{\odot} < 0.8$, or (100 deg^2/9 deg^2)×(20% complete/67% complete) for stars with $M < 0.2$ M$_{\odot}$.

Figure 6.13 shows IMFs for the low mass stellar and substellar population of the USco association. The top panel shows separately IMFs derived from the Quest-2 survey (black hatched histogram) and the Preibisch et al. (2002) survey (blue hatched histogram). Both IMFs have been scaled to 20% completeness over 100 deg^2. All histograms are shown with $\sqrt{(N)}$ errorbars. The bottom panel shows the summed IMF for the combined samples. In total, the combined IMF contains ∼300 stars with masses as high as ∼0.8 M$_{\odot}$ and as low as <0.02 M$_{\odot}$. The derived mass function rises with a slope of $dN/dM \propto M^{-1.0}$, peaks at ∼0.16 M$_{\odot}$ and then gradually falls off through the substellar regime. Thus, I find the spectroscopic IMF for USco's low mass population to be very different from the photometric IMF derived by Lodieu et al. (2007) which had a flatter slope $dN/dM \propto M^{-0.3}$ from $0.3 < M/M_{\odot} < 0.01$, and peaked at M ∼0.01 M$_{\odot}$. The total mass inferred from the spectroscopic IMF over the mass range 0.8–0.02 M$_{\odot}$ is ∼156 M$_{\odot}$. If I correct this number to account for the fact that the IMF shown here is only 20% complete, the total mass inferred is ∼780 M$_{\odot}$. Brown dwarfs ($M < 0.08$ M$_{\odot}$) account for ∼20% of objects in the combined sample, but constitute only ∼4.5% of the total mass.

6.2.3 Summary of USco Survey

I have used the HR diagram to derive mass and age distributions for the new low mass members of USco discovered as part of my Quest-2 survey (chapter 5). I generated a Monte Carlo simulation aimed at modeling the expected observed age spread given a coeval 5 Myr-old population with known observable uncertainties. From quantitative

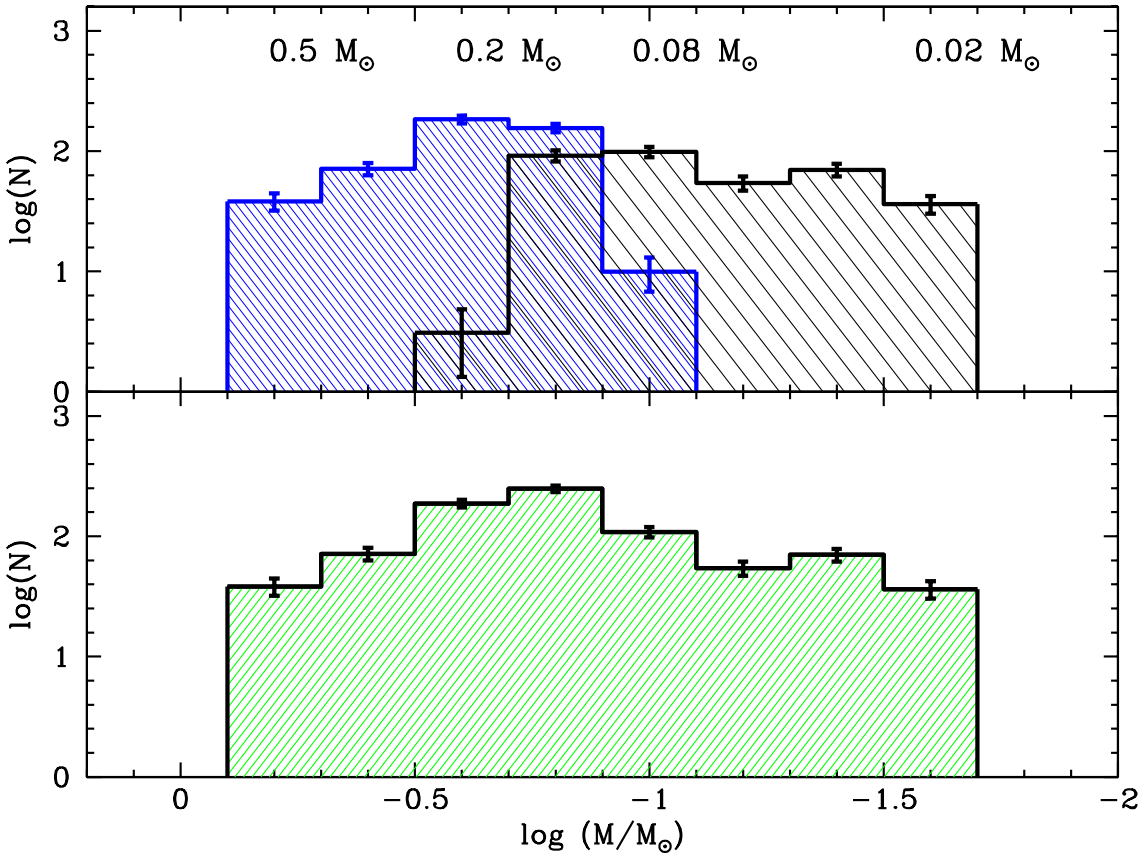

Figure 6.13 IMF for the USco association from ∼0.8–0.02 $M_\odot$. The top panel shows separately IMFs derived from the Quest-2 survey (black hatched histogram) and the Preibisch et al. (2002) survey (blue hatched histogram). Both IMFs have been scaled to a uniform 20% completeness over 100 deg^2 (see text). The bottom panel shows the cumulative IMF for the combined samples. All histograms are shown with $\sqrt{(N)}$ errorbars.

comparison of my data with simulated results I found that the data are consistent with all members of USco having formed in a single burst ∼5 Myr ago. However, if this scenario is true, the large spatial extent of the association suggests that star formation in USco was likely influenced by an external event.

I used DM97 tracks to construct the first spectroscopic IMF for USco that extends into the substellar regime. I combined my data with that from Preibisch et al. (2002) to derive a mass function with uniform completeness from ∼0.8 to 0.02 $M_{\odot}$. The derived mass function peaks at ∼0.16 $M_{\odot}$ and turns over into the brown dwarf regime.

6.3 Comparisons between Star-Forming Regions

Diagnostic studies of stellar populations in different locations and at varying stages of evolution are needed to explore the possibility of a universal mass function. While one might expect that the IMF should vary with star formation environment, we do not yet have enough evidence to determine if such a variation exists. Aside from work already mentioned in the ONC and USco, numerous studies have been carried out to characterize the low mass stellar and substellar mass functions of other young clusters in various environments. Because of the intrinsic faintness of these objects, most surveys are photometric. Authors then use a combination of theoretical models and statistical analysis to transform a cluster's color-magnitude diagram or luminosity function into an IMF which may or may not accurately represent the underlying cluster population (see §6.1.2.2).

However, the substellar populations of several other young star-forming regions have been studied spectroscopically using techniques similar to those presented here. Luhman et al. (2003b) studied the rich cluster IC 348 in Perseus, and Levine et al. (2006) studied the young cluster of NGC 2024 within the Orion Ib association. Aside from my work, there have been several additional studies of the Taurus region using similar techniques, namely those by Luhman (2000), Briceño et al. (2002), Luhman et al. (2003a), and Luhman (2004b), which together constitute a complete sample within a selected region. The data for IC 348 (Luhman et al., 2003b) and Taurus

(Luhman 2000, Briceño et al. 2002, Luhman et al. 2003a, and Luhman 2004b) are published as complete across all mass ranges within the areas surveyed. Data for NGC 2024 (Levine et al., 2006), are not complete in the magnitude range 11.25< K <14.75. These authors derived corrections in the same manner as I have employed in the ONC. The corrected values are not published; however, based on visual assessment of the published IMF from this work (see Levine et al. 2006, figure 9), the corrections appear to be uniform across all masses. Thus, for the purpose of this discussion I assume the IMF for NGC 2024 to be *relatively* complete across all masses considered. These three clusters are all young ($age \lesssim 3$ Myr), and, similar to the ONC and USco, have not yet had time to lose members through dynamical ejection. Therefore, if the IMF is universal, similar mass distributions should be observed for all five regions.

Direct comparison of the published data requires caution given that different mass tracks were used to derive masses for different studies. To avoid this problem, I have used published effective temperatures and luminosities from the studies listed above to re-derive masses for the three comparison regions with both the DM97 (D'Antona & Mazzitelli, 1997) and the BCAH98 (Baraffe et al., 1998) tracks using the same interpolation program used to derive masses for my samples in the ONC and in USco. Resultant IMFs are shown in figures 6.14 and §6.15. For the ONC and USco I have shown completeness-corrected IMFs as discussed in §6.1.2 & 6.2.2. Remarkably, for both sets of tracks I find a common turnover at the low mass end in all five regions. For the purpose of this study I will discuss only the DM97 comparative results consistent with my prior analysis, but note that varying conclusions can be drawn dependent upon which models one is using. This is a very important, but too often downplayed, caveat that must be kept in mind for any discussion regarding the low mass IMF.

From the DM97 models I find that all five star forming regions exhibit a common peak at $M \sim 0.16$ $M_{\odot}$. Note the varying scales on the y-axis (my samples in USco and the ONC have more stars than the comparison studies) and the fact that while the mass functions for USco or the ONC do not include the associated high mass stars, I have not cut these from the literature samples of IC 348 or Taurus. The Levine et al.

(2006) study in NGC 2024, similar to my work, concentrated only on the low mass stars and brown dwarfs despite the large number of high mass stars present in this cluster.

One method by which I can quantitatively examine differences between the mass distributions is to use KS tests. I ran a KS test between the mass distributions for each association. I limited the mass ranges to 0.02 $M_\odot < M < 0.5$ $M_\odot$ to account for the lack of inclusion of high mass stars for some samples. I find that the derived mass functions for three associations, USco, the ONC and NGC 2024, are consistent with being drawn from the same distribution (probabilities $\gtrsim$5%–30%). These same three associations were highly inconsistent with the distribution found for IC 348 with probabilities of <0.02% in all cases. All four associations were borderline inconsistent with the Taurus distribution at the $\lesssim$1% probability level.

Another common method employed when comparing mass distributions for different star forming regions is to compute the relative numbers of brown dwarfs to stars. However, with the possible exception of the ONC, examination of figure 6.14 reveals nothing distinguishing about the distributions on either side of the substellar limit (M=0.08 $M_\odot$; Log($M/M_\odot$)=-1.1). Thus, I have chosen to use as a divisor the peak of the mass function, which is more physically significant in this case than the substellar limit. I will define my high mass bin to be limited to stars <0.5 $M_\odot$ because several of the mass functions presented here do not include high mass stars above this limit. All surveys are complete (within the area surveyed) through $M \sim$0.02 $M_\odot$. I have computed the ratio R_N defined as:

$$R_N = \frac{N(-1.7 \leq log(M/M_\odot) \leq -0.9)}{N(-0.9 < log(M/M_\odot) \leq -0.3)}$$

for each of the five mass distributions. I find relatively small R_N values for Taurus and IC 348, 0.24 and 0.17, respectively. For the other three associations I find much higher values of 0.53 (NGC 2024), 0.64 (ONC – corrected for uniform completeness), 0.58 (ONC – raw data), 0.49 (USco – corrected for uniform completeness), and 0.62 (USco – raw data). Using a two-tailed Fisher's Exact test on the raw data for all five

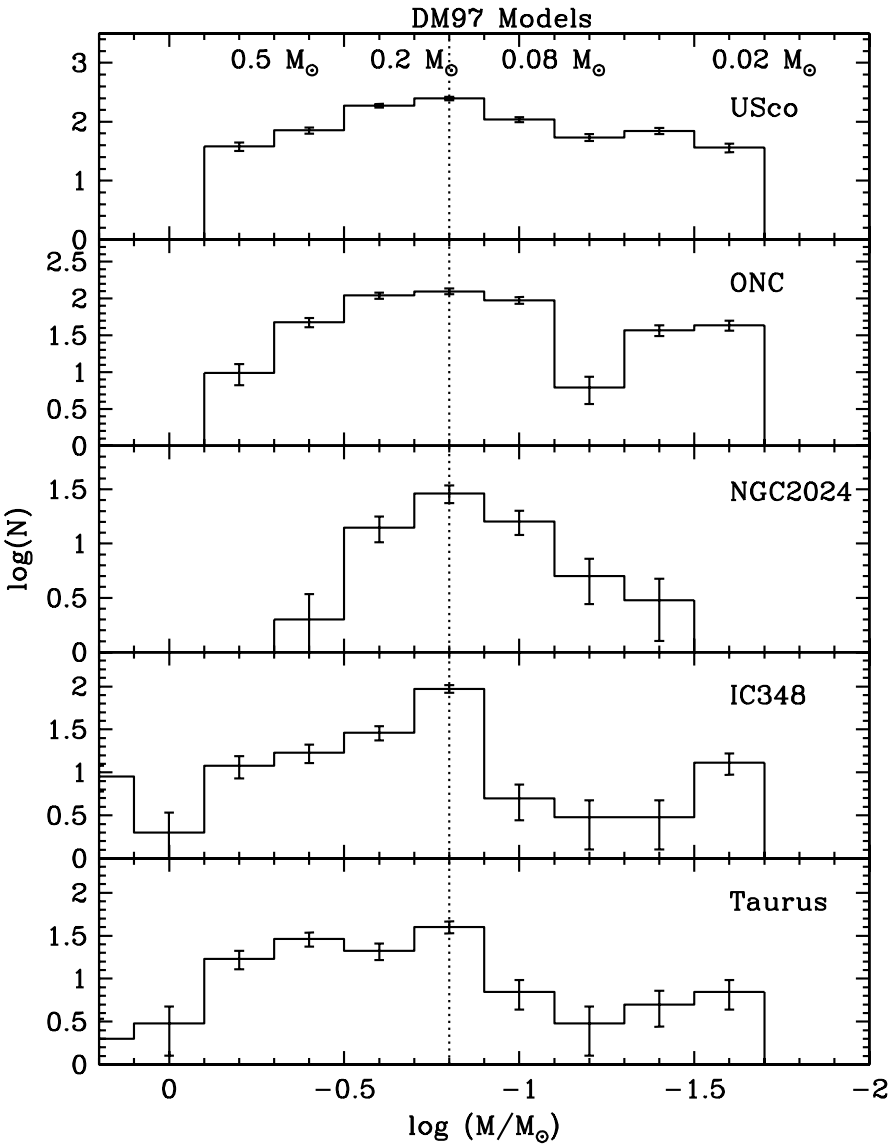

Figure 6.14 Low mass IMFs for USco, the ONC, NGC 2024, IC 348, and Taurus generated from DM97 mass tracks. Data for the latter three regions were taken from the literature (see text). I find a common peak a M $\sim$0.16 $M_{\odot}$ for all five regions and then a turn over into the substellar regime, the form of which may vary.

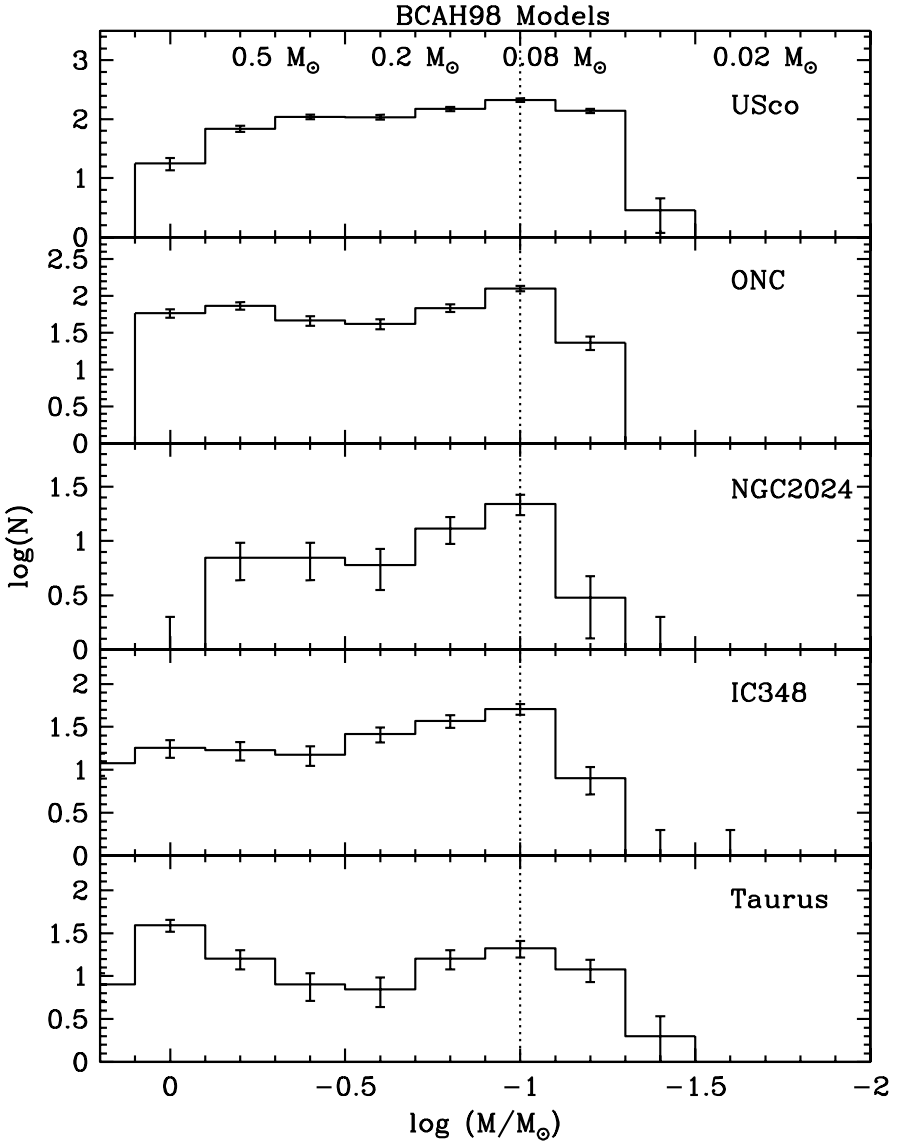

Figure 6.15 Low mass IMFs for USco, the ONC, NGC 2024, IC 348, and Taurus generated from BCAH98 mass tracks. Data for the latter three regions were taken from the literature (see text). As for the IMFs generated from DM97 tracks (figure 6.14), I find a common peak for all regions (though in Taurus this may be a secondary peak). However, using the BCAH98 tracks the peak is shifted to lower mass (M $\sim$0.1 $M_{\odot}$) than that found using the DM97 tracks.

mass functions, I compute that the measured R_N values for NGC 2024, USco, and the ONC are consistent with each other at the 70%–80% level, and different from the R_N values for IC 348 with $\lesssim$0.1% probability that the R_N values could have been drawn from the same distribution. Comparison of R_N values for NGC 2024, USco and the ONC with that for Taurus finds $\lesssim$4% probability of consistency in all cases. These correlations, together with results from the KS tests, strongly suggests that there is something similar about the mass distributions for NGC 2024, the ONC and USco that is not found for IC 348 and Taurus.

While the environments of the ONC and NGC 2024 are similar, they are different from that of USco in that USco is a low stellar-density, OB association rather than a high stellar-density embedded cluster. One factor, however, that all three former regions have in common which IC 348 and Taurus do not share is the presence of hot, ionizing stars. The young regions of NGC 2024 and the ONC, both have an O-type member. The older region of USco currently has 49 B-type stars and its most massive member, the O7-type progenitor of pulsar PSR J1932+1059 exploded as a supernova $\sim$1.5 Myr ago (de Geus, 1992). Conversely, neither Taurus nor IC348 have (or show any evidence for having once had) a member earlier than $\sim$B5 (Briceño et al. 2002, Luhman et al. 2003b). It is possible that a prestellar core in the presence of an ionizing OB (i.e., with spectral type earlier than $\sim$B0) star may ultimately become a lower mass star than it otherwise would have because much of its surrounding material is eroded away by ionizing radiation before it can be accreted. This scenario has been discussed previously in the literature both through observational arguments (e.g., Robberto et al. 2004; Luhman 2004b) and through quantitative theoretical analysis (e.g., Whitworth & Zinnecker 2004; Kroupa & Bouvier 2003). However, this process for generating low mass stars can only take place during the first $\sim 10^5$ yr of a protostar's lifetime when most of its material in still in an accretion envelope, and will only significantly affect cores close to ($\lesssim$1 pc, dependent on the mass of the ionizing star) the source of ionization (Kroupa & Bouvier, 2003). Thus, this mechanism may be responsible (at least in part) for the larger numbers of low mass stars and brown dwarfs seen in the two clustered regions of the ONC and NGC 2024,

however, it likely can not have affected protostellar cores across the entire ∼35 pc expanse of USco. These arguments do not, however, exclude the possibility that some other mechanism inherent to regions with high mass stars in some way causes larger numbers of associated low mass stars. For example, Adams et al. (2006) have shown through numerical simulation that disks around lower mass stars are more susceptible to destruction (further out than ∼10 AU) from interactions with surrounding stars of higher mass. It is possible that in a similar manner, low mass cores moving through a giant molecular cloud are more susceptible to being stripped of their accretion envelope in the presence of higher mass cores.

In conclusion to this section, I have re-derived mass functions for the low mass stellar and substellar populations of five recently star forming regions using a consistent set of mass tracks and a common interpolation scheme. Remarkably, I find a common peak for all five regions using either the DM97 or the BCAH98 tracks, implying the IMF turnover may be independent of environment. Based on masses derived from the DM97 tracks, I find that mass distributions for the three regions containing high mass stars, the ONC, NGC 2024 and USco, are statistically consistent with each other, but significantly different from the mass distributions for the two regions Taurus and IC 348 which do not contain OB stars. This result is supported by the finding that the three former associations contain several times more very low mass stars and brown dwarfs compared to stars with masses greater than the IMF turnover than do the latter two. Both results suggest that, within a star forming region, the presence of very massive stars may play a large role in determining the low mass IMF.